Dyes and Pigments 241 (2025) 112881

Contents lists available at ScienceDirect

Dyes and Pigments

journal homepage: www.elsevier.com/locate/dyepig

Supramolecular Aggregates from core-functionalized 1,8-naphthalimides: insights into self-assembling and sensing ability for drugs in water

Salvatore Marullo, Eleonora Capuano, Francesca D'Anna *

Università degli Studi di Palermo, Dipartimento di Scienze Biologiche, Chimiche e Farmaceutiche, Viale delle Scienze, Ed. 17, 90128, Palermo, Italy

ARTICLE INFO

Keywords:
1,8-Naphthalimide
Self-assembly
Fluorescent sensing
Drugs

ABSTRACT

To monitor emerging pollutants in water, we herein describe three novel core-substituted, self-assembling 1,8-naphthalimide derivatives, applied as fluorescent sensors to detect drugs in water. These fluorophores differ for the substitution on the core and imide positions. We initially studied photophysical properties of the fluorophores by solvent-dependent UV–vis and fluorescence measurements and then investigated their self-assembly, finding that they mostly form *J*-aggregates in water and water/DMSO solutions, following an isodesmic pathway. We also obtained insights on the thermodynamic parameters of the aggregation process and characterized the aggregate morphology by Scanning Electron Microscopy. Subsequently, we studied how these supramolecular aggregates act as fluorescent sensors to detect in aqueous solutions drugs belonging to different classes, like non-steroidal, anti-inflammatory and antibiotic drugs. To this aim, we conducted fluorescence measurements in the presence of variable drug concentrations. The best-performing system could detect ketoprofen with limit of detection (LOD) and limit of quantification (LOQ) of 2.3 and 6.9 μM, respectively. Finally, we embedded the best-performing fluorophore onto solid supports including filter paper strips or polymer poly(3-hydroxybutirate) films. When these fluorophore-doped solids were soaked in ketoprofen solutions at different concentrations, significant quenching of emission was detected.

1. Introduction

Monitoring water quality is an unavoidable task to ensure acceptable standards of living, and this is pursued in most of the world with dedicated regulations. However, the last decades have seen the increasingly concerning issues of emerging pollutants, i.e. harmful substances, not yet comprised in regulations and analysis protocols for water bodies [1]. Among these pollutants, drug residues elicit particular concerns [2]. Deriving from multiple sources, like households, healthcare centers or livestock production facilities, drugs in water bodies pose significant risk to both aquatic organisms and human health [3–5]. Drugs are often resistant to conventional water treatment methods and, in addition, can be present at different concentrations, spanning a wide range of structures. These considerations motivate research to find fast and efficient methods to detect the presence of drugs in water. Among the various methods that can be used to track the presence of pharmaceutically active compounds in water, like cyclic voltammetry, chromatography, capillary electrophoresis or mass spectroscopy [6,7], fluorescent sensing appears particularly suitable. This is due to the ability of fluorescent sensing to detect analytes at very low concentrations, coupled with the advantages of fast response, possibility of *in situ* detection without need of expensive instrumentation, transportation or sample pretreatment [8].

Fluorescent chemosensing is generally driven by non-covalent interactions established between the analyte and a fluorescent probe, which induce significant variations in the emission of this latter. A number of mechanisms can be involved in this process, such as fluorescence turn-on, turn-off or photoinduced electron transfer [9].

Consequently, different supramolecular interactions can be harnessed to detect pharmaceutically active compounds in water environment at low concentrations, and systems based on metal organic frameworks [10], macrocyclic hosts [11,12] and fluorophores functionalized with selective receptor units have been reported [13].

A further related sensing strategy involves using supramolecular aggregates as sensory probes [14,15].

In such an approach, emission variations of supramolecular aggregates formed by a suitable fluorescent monomer, are induced by the presence of the analyte. Hence, this strategy often involves very simple

* Corresponding author.
E-mail address: francesca.danna@unipa.it (F. D'Anna).

https://doi.org/10.1016/j.dyepig.2025.112881
Received 20 January 2025; Received in revised form 6 May 2025; Accepted 7 May 2025
Available online 19 May 2025

molecules, and has been applied for the obtainment of ultrasensitive sensors. In this respect, a metal-ion containing supramolecular gel has been successfully used for the detection of [$H_2PO_4^-$] anion in water [16], or supramolecular aggregates formed by peptides were reported for the sensing of a melanoma biomarker [17]. In addition, aggregates formed by perylene diimide derivatives provided sensory platforms for sensitive detection of metal ions [18] or berberine chloride [19].

An important class of fluorescent and aggregating compounds is constituted by 1,8-naphthalimide (NI) derivatives. These molecules often form emissive aggregates in solution, underpinned by π -π stacking interactions [20]. Notably, despite the well-known self-assembling ability of NI-derivatives, the use of NI-based aggregates for pollutant sensing is relatively underexplored, compared with other kinds of applications, featuring sensing of harmful gases [21], metals [22] in solution as well in gel state [23]. In this context, we have demonstrated that the emission of such aggregates can be exploited for bioimaging applications [24], and very recently, that supramolecular aggregates based on a D-glucamine functionalized NI-fluorophore, can act as fluorescent sensor for the detection of drugs in aqueous solutions [25]. Notably, functionalization of the core positions in NI-derivatives greatly influence, and in many cases enhances, the emission ability [26]. It is indeed widely reported that substitution of the 4-position of the aromatic core of 1,8-naphthalimides with different groups, including amino groups, significantly alter the electronic distribution in the fluorophore, thus affecting UV–vis and fluorescence properties [27–29]. Substitution with secondary amine groups such as piperidyl can potentially reduce the extent of π-stacking, responsible for ACQ phenomena [30]. Since π-stacking mainly underpins the self-assembly of 1,8-naphthalimides derivatives, this structural variation can also affect the stability of the aggregates formed.

Based on these considerations, we synthesized three NI-based fluorophores, differently functionalized on both in the aromatic rings and imide positions, namely **Pyrr-NI-Im**, **Pyrr-NI-Glu**, and **Mor-NI-Im** (Fig. 1).

In particular, the different functionalization on the aromatic core is expected to affect the emissive profile of the fluorophore, while the different groups in the amide moiety should influence the aggregation of the NI-nuclei. More specifically, the alkyl-imidazole moiety provides the NI-based fluorophores with further π-conjugated surface, thus in principle enhancing π-π interactions [20]. On the other hand, the introduction of the D-glucamine moiety has been reported to increase solubility in water and favour aggregation, due to the presence of additional hydrogen bonding sites [31,32].

We investigated the self-assembly process of each fluorophore by concentration- and temperature dependent UV–vis and fluorescence measurements in water, while the morphology of the aggregates was probed by Scanning Electron Microscopy (SEM). We also studied the photophysical properties of the fluorophores in different solvents, also in the solid state. Then, we employed the aggregates of each fluorophore in water or, for solubility reasons, water/DMSO mixtures, to detect the presence of the drugs reported in Fig. 1. In particular, we chose drugs of different classes, like ketoprofen and diclofenac sodium salt commonly used as non-steroidal anti-inflammatory drugs, antibiotics like nalidixic acid and ciprofloxacin, as well as the anticonvulsant carbamazepine. Regarding their structure, ketoprofen has a carboxylic acid group, while diclofenac is a carboxylate salt. Furthermore, carbamazepine has the highest molecular rigidity, while ciprofloxacin and nalidixic acid in aqueous solutions are mainly present in aqueous solutions in the zwitterionic form. We conducted this investigation by fluorescence emission measurements of solutions containing a fixed concentration of fluorophore and increasing amounts of drugs, to obtain the limits of detection (LOD) and quantification (LOQ). The best-performing system, **Pyrr-NI-Im,** could detect ketoprofen with limit of detection (LOD) and limit of quantification (LOQ) of 2.3 and 6.9 μM, respectively.

For this latter, we also explored the possibility of embedding it in paper strips or polymer membrane, to sense the presence of ketoprofen in solution, finding significant quenching on increasing drug concentration.

2. Experimental section

2.1. Materials

4-Chloro-1,8-naphthalic anhydride, 1-(3-aminopropyl)imidazole, pyrrolidine, morpholine, poly-(3-hydroxybutirate), D-glucamine, diethylene glycol dimethyl ether and all the solvents used were obtained from commercial sources and used without further purification.

2.2. Synthesis of the fluorophores

The fluorophores were synthesized by suitably modified reported procedures [29,33].

2.2.1. General procedure for the synthesis amino-substituted 1,8-naphthalic anhydride precursors

In a round-bottom flask, 4-chloro-1,8 naphthalic anhydride (1.5 g, 6.5 mmol) and 1.4 equivalents of amine were dissolved in diethylene glycol dimethyl ether (10 mL), and the resulting mixture was kept at 140 °C, for 48 h, under stirring. Subsequently, the reaction mixture was cooled down at room temperature, the brown precipitate was filtered off and then washed with portions (4 × 5 mL) of cold deionized water. The resulting solid was purified by column chromatography on silica, employing dichloromethane as eluent. The product was obtained as an orange solid, after removal of the solvent by evaporation at reduced pressure.

2.2.2. 4-(N-pyrrolidyl)-1,8 naphthalic anhydride (Pyrr-NI)

Orange solid. Yield: 45 %; ^{1}H NMR (400 MHz, $CDCl_3$) δ: 2.02 (m, 4H), 3.81 (t, $J = 8.0$ Hz, 4H), 6.90 (d, $J = 8.0$ Hz, 1H), 7.64 (dd, $J_1 = 8.0$ Hz, $J_2 = 7.2$ Hz, 1H), 8.22 (d, $J = 8.0$ Hz, 1H), 8.43 (d, $J = 8.0$ Hz, 1H),

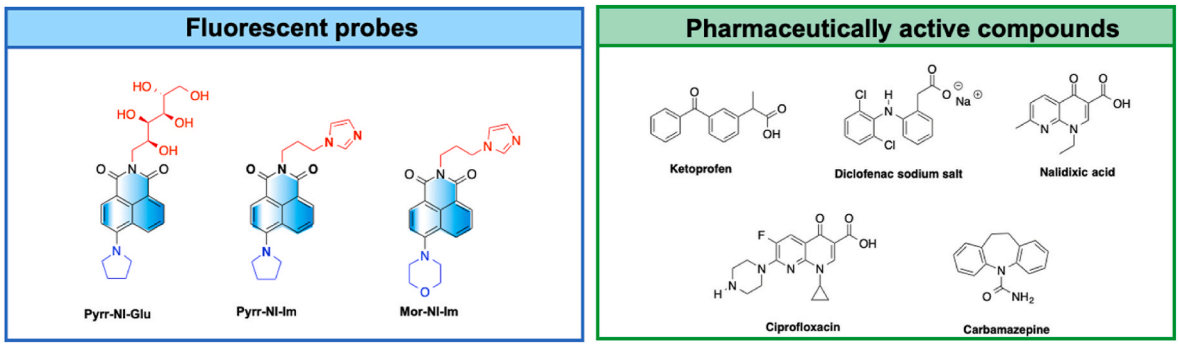

Fig. 1. Structures of fluorescent probes and drugs considered.

8.83 (d, $J = 8.0$ Hz, 1H). FT-IR (nujol mull): 1740 (C═O), 1696 (C═O) cm^{-1}.

2.2.3. 4-(N-morpholyl)-1,8 naphthalic anhydride (Mor-NI)

Orange solid. Yield: 38 %; ^{1}H NMR (400 MHz, $CDCl_3$) δ: 3.33 (t, $J = 8.0$ Hz, 4H), 4.04 (t, $J = 8.0$ Hz, 4H), 7.25 (d, $J = 8.0$ Hz, 1H), 7.74 (dd, $J_1 = 8.4$ Hz, $J_2 = 7.2$ Hz, 1H), 8.47 (dd, $J_1 = 8.4$ Hz, $J_2 = 0.4$ Hz, 1H), 8.51 (d, $J = 8.0$ Hz, 1H), 8.57 (dd, $J_1 = 7.2$ Hz, $J_2 = 0.4$ Hz, 1H) ppm. ^{13}C NMR (400 MHz, $CDCl_3$) δ (ppm): 53.3, 66.8, 112.3, 115.2, 119.5, 126.1, 126.2, 131.6, 132.2, 133.3, 134.8, 156.8, 160.4, 161.1 ppm.

2.3. General procedure for the synthesis of NI-based fluorophores by imidation of precursors

2.3.1. Pyrr-NI-Im

In a sealed vessel, (0.67 g, 2.5 mmol) of Pyrr-NI was dissolved in toluene (35 mL), heating at 110 °C, under stirring for 30 min. To the resulting solution, a solution of 1-(3-aminopropyl) imidazole (0.37 g, 3.0 mmol) in 15 toluene (15 mL) was added dropwise. The resulting mixture was kept at 110 °C for 72 h, under stirring. Subsequently, the reaction mixture was cooled down at room temperature, and the orange precipitate was filtered off. The solid obtained purified by column chromatography using dichloromethane/methanol 20/1 (v/v) as eluting mixture. The solid obtained from the combined fractions, after removal of the solvent, was further suspended in acetone, and subjected to sonication for 5 min. The supernatant layer of solvent was decanted and the solid was dried at reduced pressure, obtaining 0.57 g of a red-orange solid.

Yield: 61 %; m.p.: 100 °C; ^{1}H NMR (400 MHz, $CDCl_3$) δ: 2.11 (m, 4H), 2.26 (quin, $J = 8.0$ Hz, 2H), 3.79 (m, 4H), 4.07 (t, $J = 8.0$ Hz, 2H), 4.24 (t, $J = 8.0$ Hz, 2H), 6.81 (d, $J = 8.0$ Hz, 1H), 7.04 (m, 2H), 7.54 (dd, $J_1 = 8.0$ Hz, $J_2 = 0.4$ Hz 1H), 7.58 (bs, 1H), 8.41 (d, $J = 16.0$ Hz, 1H), 8.56 (d, $J = 8.0$ Hz, 1H), 8.60 (d, $J = 8.0$ Hz, 1H) ppm. ^{13}C NMR (400 MHz, DMSO) δ: 26.1, 29.8, 37.3, 45.2, 53.2, 106.6, 110.2, 118.8, 122.2, 122.5, 123.05, 129, 131.2, 132.2 (2C overlapped), 133.6, 137, 152.8, 164, 164.9 ppm. FT-IR (nujol mull): 1635 cm^{-1} (C═O) 1685 cm^{-1} (C═O). Elemental analysis (%) calcd. for $C_{22}H_{22}N_4O_2$: C 70.57, H 5.92, N 14.96; found: C 70.23, H 6.29, N 14.75.

2.3.2. Mor-NI-Im

In a sealed vessel, Mor-NI (0.35 g, 1.2 mmol) was dissolved in toluene (25 mL), heating at 110 °C under stirring for 30 min. To the resulting solution, a solution of 1-(3-aminopropyl)imidazole (0.18 g, 1.5 mmol) in toluene (5 mL) was added dropwise. The resulting mixture was kept at 110 °C for 72 h, under stirring. Subsequently, the reaction mixture was cooled down at room temperature and the precipitate was filtered off, obtaining 0.39 g of an orange needle-like solid.

Yield: 83 %; m.p.: 155–157 °C; ^{1}H NMR (400 MHz, $CDCl_3$) δ: 2.27 (quin, $J = 8.0$ Hz, 2H), 3.28 (t, $J = 8.0$ Hz, 4H), 4.03 (t, $J = 8.0$ Hz, 4H), 4.09 (t, $J = 8.0$ Hz, 2H), 4.24 (t, $J = 8.0$ Hz, 2H), 7.04 (dt, $J_1 = 12.0$ Hz, $J_2 = 0.8$ Hz, 2H), 7.25 (d, $J = 8.0$ Hz, 1H), 7.61 (s, 1H), 7.72 (dd, $J_1 = 8.8$ Hz, $J_2 = 7.6$ Hz, 1H), 8.44 (dd, $J_1 = 7.6$ Hz, $J_2 = 1.2$ Hz, 1H), 8.54 (d, $J = 8.0$ Hz, 1H), 8.60 (dd, $J_1 = 7.6$ Hz, $J_2 = 1.2$ Hz, 1H) ppm. ^{13}C NMR (400 MHz, $CDCl_3$) δ: 29.7, 37.6, 45.0, 53.4, 63.9, 115.0, 116.7, 118.7, 123.0, 125.9, 126.1, 129.5, 129.9, 130.4, 131.4, 132.8, 137.1, 155.9, 164.0, 164.5 ppm. FT-IR (nujol mull): 1647 cm^{-1} (C═O) 1686 cm^{-1} (C═O). Elemental analysis (%) calcd. for $C_{22}H_{22}N_4O_3$: C 67.68, H 5.68, N 14.35; found: C 66.30, H 6.01, N 14.19.

2.3.3. Pyrr-NI-Glu

In a sealed vessel, Pyrr-NI (0.2 g, 0.75 mmol), D-glucamine (0.14 g, 0.75 mmol) and DMF (20 mL) were added, and the resulting mixture was kept at 110 °C for 72 h, under stirring. Subsequently, the reaction mixture was cooled down at room temperature, the solvent was evaporated at reduced pressure and the ensuing residue was suspended in methanol (100 mL). Then, the supernatant layer of solvent was decanted and the solid was dried at reduced pressure. This latter was purified by column chromatography on silica, using dichloromethane/methanol 10/1 (v/v) as eluting mixture, obtaining 0.17 g of an orange solid.

Yield: 49 %; m.p. > 250 °C; ^{1}H NMR (400 MHz, D_6-DMSO) δ: 2.01 (m, 4H), 3.39 (m, 1H), 3.47 (m, 2H), 3.57 (d, $J = 8.0$ Hz, 1H), 3.64 (m, 1H), 3.76 (m, 4H), 3.98 (m, 2H), 4.32 (m, 3H), 4.40 (m, 1H), 4.49 (m, 1H), 4.64 (d, $J = 8.0$ Hz, 1H), 6.88 (d, $J = 12.0$ Hz, 1H), 7.61 (t, 1H), 8.24 (d, $J = 8.0$ Hz, 1H), 8.42 (d, $J = 8.0$ Hz, 1H), 8.73 (d, $J = 8.0$ Hz, 1H). ^{13}C NMR (400 MHz, DMSO) δ: 26.0, 43.1, 53.3, 63.8, 70.3, 70.8, 71.9, 73, 108.9, 109.6, 122.3, 123.7, 124.9, 131, 132.9, 133.4, 152.6, 163.8, 164.7 ppm. FT-IR (nujol mull): 1636 cm^{-1} (C═O). Elemental analysis (%) calcd. for $C_{22}H_{26}N_2O_7$: C 61.39, H 6.09, N 6.51; found: C 60.09, H 6.87, N 6.24.

2.4. UV–vis and fluorescence spectroscopy measurements

Samples for UV–vis and fluorescence spectroscopy were prepared by dilution of stock solutions in dichloromethane, for **Pyrr-NI-Im** and **Mor-NI-Im**, and in methanol for **Pyrr-NI-Glu**. The suitable volume of solution was transferred in a vial and the solvent was evaporated at reduced pressure. Then, the residue was dissolved in 2 mL of the opportune solvent. All the solutions were limpid after this treatment. UV–vis spectra were recorded at 25 °C on a Beckmann DU800 spectrophotometer equipped with a Peltier temperature controller, employing quartz cuvettes with 1 cm optical path.

Samples for fluorescence spectroscopy were degassed prior to measurement. Spectra were recorded with a JASCO spectrofluorometer using quartz cuvettes with 0.2 cm optical path and λ_{exc} was set at the maximum absorbance wavelength, while excitation and emission bandwidths were set at 2.5 nm.

Acidic and basic solutions employed for p*H*-dependent fluorescence measurements were obtained by additions of HCl and NaOH.

Relative fluorescence quantum yields were determined by a reported procedure [34]. Quantum yields were determined at 25 °C, relative to 9, 10-diphenylanthracene in ethanol or sodium fluorescein in NaOH 0.1 M, employing the standard quantum yield values reported in the literature [35].

2.5. SEM images

Samples for SEM images were prepared by casting on an aluminum stub 50 μL of an aqueous solution of each fluorophore, and the solvent was removed by evaporation at room temperature. Then, SEM images were recorded on a PRO X PHENOM electronic scanning microscope, operating at 5 KV.

2.6. Solid state fluorescence spectra

Solid-state fluorescence spectra were recorded from films obtained by casting 200 μL of water solutions of fluorophore ($1.0 \cdot 10^{-5}$ M for **Pyrr-NI-Im** and **Pyrr-NI-Glu** or $2.0 \cdot 10^{-5}$ M for **Mor-NI-Glu**) onto quartz plates. The solvent was removed by evaporation at room temperature, obtaining a solid thin film. To ensure a meaningful comparison between solid- and solution phase spectra, the excitation spectra were recorded for each sample. Emission spectra were obtained by exciting the samples at the λ_{max} obtained by excitation spectra.

2.7. Fluorescence sensing of drugs

Sensing measurements for the detection of drugs in aqueous solutions were carried out by recording fluorescence spectra of solutions containing a fixed amount of fluorescent probe ($1.0 \cdot 10^{-5}$ M for **Pyrr-NI-Im** as well as **Pyrr-NI-Glu** or $2.5 \cdot 10^{-5}$ M for **Mor-NI-Glu**) and increasing amounts of drugs. Drug concentrations were comprised between $1.0 \cdot 10^{-7}$ M and $9.0 \cdot 10^{-5}$ M. Solutions were prepared by dilution of stock solutions as previously described. For each measurement, at least 30

solutions were prepared and the relevant emission spectra were obtained as described above. Then, for each sample, the ratio I/I_0 was determined where I_0 is the maximum intensity emission of the solution containing no drug and I is emission intensity in the presence of a given amount of drug. This ratio was plotted as a function of the concentration of drug and, whenever present, the linear tract of this plot was fitted by linear regression analysis, to obtain the limit of detection (LOD) and the limits of quantification (LOQ) [36], by means of Eqs. (1) and (2):

$$LOD = 3 \cdot S_y/s \quad (1)$$

$$LOQ = 10 \cdot S_y/s \quad (2)$$

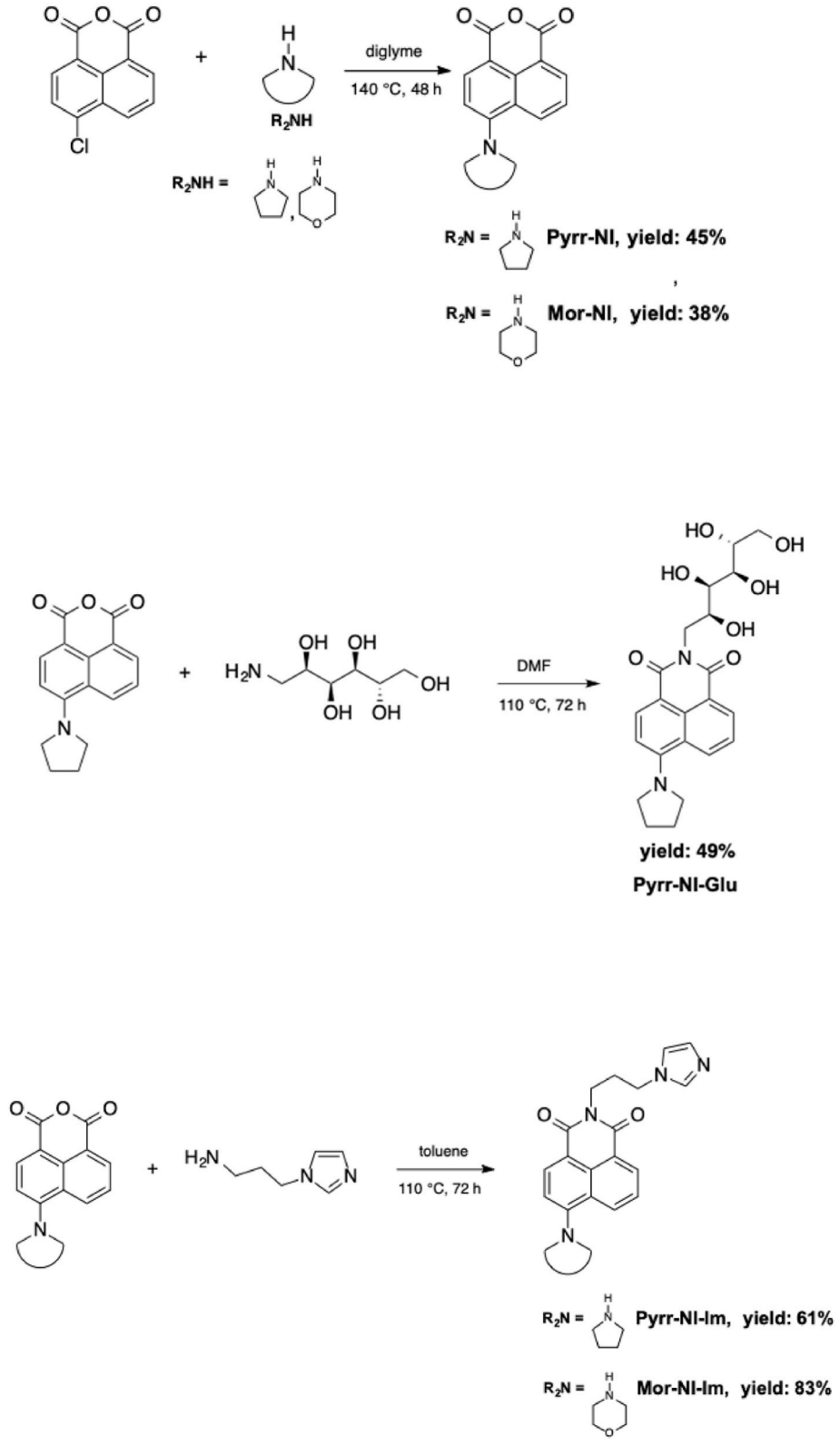

Fig. 2. Synthesis of the fluorescent probes.

where S_y is the error on the intercept and s is the slope of the curve.

2.8. Fluorescence sensing test on filter paper strip

Two strips of filter paper (2 cm × 2 cm) were soaked in 5 mL of a $1.0{\cdot}10^{-5}$ M of **Pyrr-NI-Im** in dichloromethane for 5 min. Then, the strips were withdrawn and the solvent was evaporated at room temperature for 24 h. Then, the excitation and emission spectra of the strips were recorded. Subsequently, the strips were immersed for 5 min in Petri dishes containing 5 mL of water solutions of ketoprofen at concentrations of $4.8{\cdot}10^{-6}$ M, $1.3{\cdot}10^{-5}$ M respectively. Subsequently, the strips were removed and dried at room temperature for 24 h. Finally, the emission spectra of each strip were recorded. Spectra were obtained setting the excitation and emission bandwidth slits at 2.5 nm, at λ_{exc} = 439 nm.

2.9. Fluorescence sensing test on polymer membrane

Poly(3-hydroxybutirate) (0.5 g) was dissolved in chloroform (12 mL) in a vial and heated at 50 °C for 40 min, under stirring. To the resulting solution, a $1.0{\cdot}10^{-5}$ M chloroform solution of **Pyrr-NI-Im** (5 mL) was added, stirring for further 5 min. Subsequently, the entire solution was transferred in a Petri dish and the solvent was evaporated at room temperature. A colorless membrane was obtained, and the excitation and emission spectra were recorded. Subsequently, an aqueous solution of ketoprofen ($2.5{\cdot}10^{-5}$ M) was prepared and a rectangular section (2 cm × 2 cm) of the fluorophore-doped membrane was soaked in 5 mL of drug solution for 2 min. The membrane was removed and dried at room temperature for 24 h. Finally, the emission spectra of the membrane were recorded. Spectra were obtained setting the excitation and emission bandwidth slits at 2.5 nm, at λ_{exc} = 444 nm.

3. Results and discussion

3.1. Synthesis of fluorophores

All the fluorophores were prepared by a two-step synthesis, depicted in Fig. 2, by modifications of previously reported procedures for the functionalization of similar nuclei [24,37–41].

In the first step, we functionalized the aromatic core, by nucleophilic aromatic substitution on 4-chloro-1,8-naphthalic anhydride with the secondary amines pyrrolidine and morpholine. Then, we reacted the anhydrides obtained with either D-glucamine or 1-(3-aminopropyl) imidazole, to obtain the relevant naphthalimides, in good to high yields. As previously mentioned, the insertion of the D-glucamine moiety should improve water solubility and concomitantly affect the self-assembling ability [32], while the imidazole moiety can improve the propensity for aggregation, providing additional sites for π-interactions.

3.2. Photophysical properties of the fluorophores

Firstly, we investigated the photophysical properties of the fluorophores, by carrying out solvent-dependent UV–vis and fluorescence measurements. To this aim, we recorded the UV–vis and fluorescence spectra of solutions containing a fixed concentration of fluorophores, in different solvents. These solvents were chosen to span a wide range of polarity, from chloroform to water, comprising either aprotic or protic solvents. The spectra relevant to **Pyrr-NI-Im** are shown in Fig. 3a, while the ones obtained for the other fluorophores are reported in Fig. A1. In addition, Stokes shifts are reported in Table A4.

Examining the spectra reported in Fig. 3a clearly show a pronounced dependence of the absorption of **Pyrr-NI-Im** on the nature of the solvent, especially for the position of the absorption band, while no obvious change in the shape of the spectra occurs. More specifically, λ_{max} appears to shift at longer wavelength on increasing solvent polarity as can be seen from the shift from 440 nm to 447 nm on going form dichloromethane to acetone, or from 447 nm to 465 nm on going from acetone to water/DMSO 95 vol%. To gain a better understanding of the trend of absorption maximum on solvent polarity, we plotted λ_{max} as a function of the relative dielectric constant of the solvents [42,43]. The plot is reported in Fig. 3b, while the values are reported in Table A1.

Examination of the plot reported in Fig. 3b brings out a clear positive solvatochromism for **Pyrr-NI-Im**, with λ_{max} increasing with dielectric constant in an almost linear fashion. Positive solvatochromism has been previously reported for other NI-derivatives [44,45], and derives from better stabilization of the excited state relative to the ground state, on increasing solvent polarity [46].

The only deviations from this trend can be observed for the halogenated solvents chloroform and dichloromethane, whereas in protic solvents like ethanol and methanol, also a bathochromic shift on increasing polarity can be observed. Hence, the factors that appear to move the maximum absorption wavelength to higher values are the presence of protic and polar solvents. Similar conclusion can be drawn for the other fluorophores. In particular, in the case of **Pyrr-NI-Glu**, λ_{max} increased from 445 nm to 461 on going from the least polar solvent, chloroform, to water which is the most polar one (Fig. A1c), with a clear positive solvatochromism (Fig. A1d). Finally, moving to **Mor-NI-Im,** we observe an analogous trend, although variations of λ_{max} with polarity span a narrower range, as it changes from 388 nm to 400 nm on going from hexane to water. Hence, the magnitude of Δλ is influenced the substitution on the core-as well as the imide positions. Subsequently, we turned our attention to the fluorescence emission spectra of the fluorophores, recorded at constant concentration in different solvents. The spectra relevant to **Pyrr-NI-Im** are reported in Fig. 4a, while the other ones are shown in Figure A2-3. In addition, in Fig. 4c and A2-3, we report representative pictures of the sample solutions, irradiated under UV light, while the values of λ_{max} and dielectric constants are reported in Table A2.

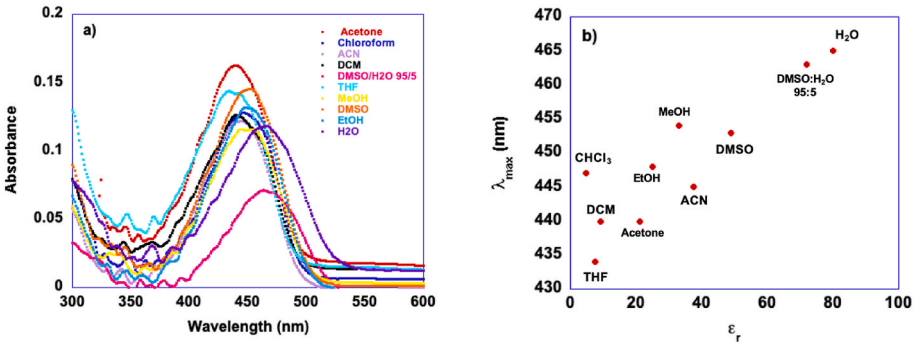

Fig. 3. a) Superimposed UV–vis spectra of **Pyrr-NI-Im** ($2.8 \cdot 10^{-5}$ M) in different solvents and b) plot of λ_{max} as a function of solvent relative dielectric constant for the same solutions.

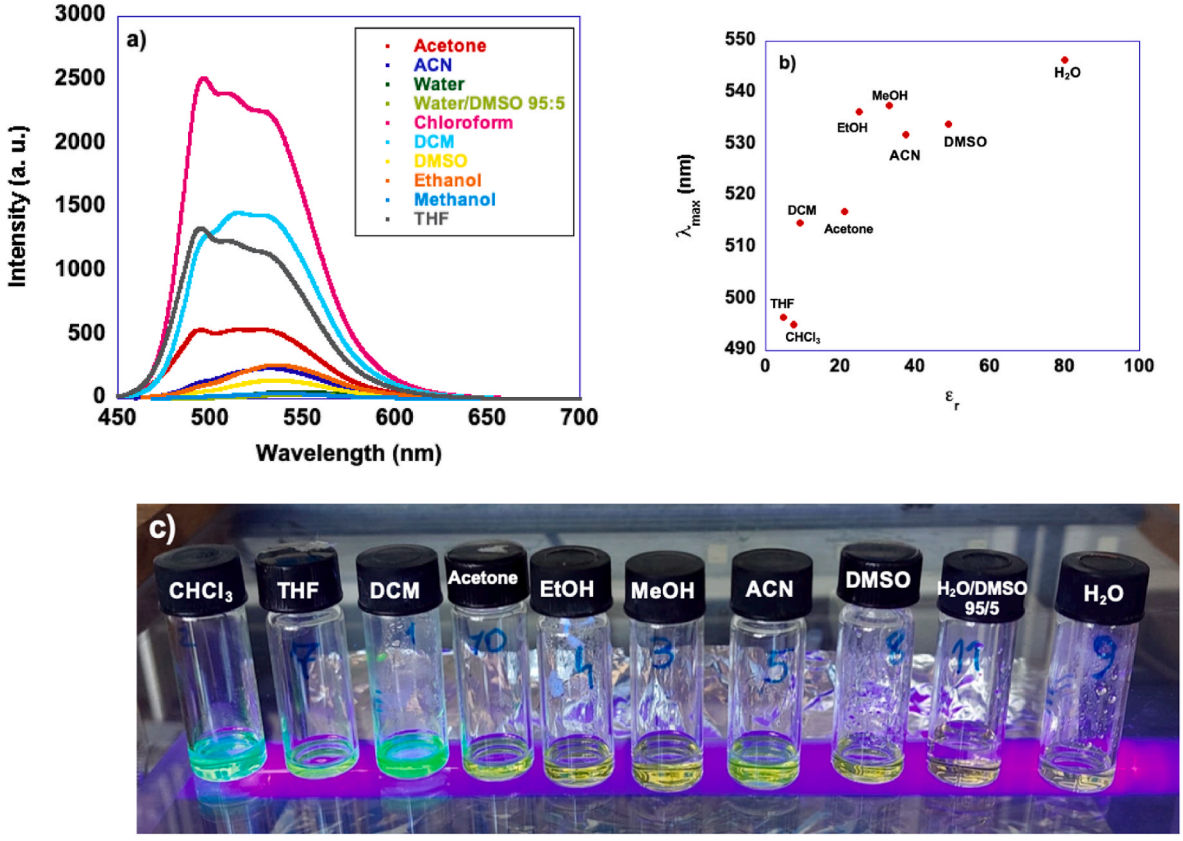

Fig. 4. a) Superimposed fluorescence spectra of **Pyrr-NI-Im** ($3.0 \cdot 10^{-6}$ M) in different solvents, b) plot of λ_{max} as a function of solvent relative dielectric constant and c) representative picture of the sample solutions irradiated under UV light.

Looking at the spectra reported in Fig. 4a, it is easy to notice that emission intensity increases significantly on going from highly polar to low polar solvents, like water and chloroform. In addition, changing the solvent induces also a variation in the shape of the spectrum which passes from the single emission band, centered at 547 nm, to a broader band, suggestive of the superposition of more emission bands in chloroform. A pronounced dependence of the value of λ_{max} on solvent polarity can also be found, as evidenced by the plot in Fig. 4b. The loss of fine structure of the emission spectrum on increasing solvent polarity, and particularly in water, can suggest the occurrence of aggregation [47, 48].

In the case of the fluorescence spectra of **Pyrr-NI-Glu**, in all solvents a single band, with no appreciable fine structure can be observed, centered in the range 520 nm ÷ 540 nm, with a shoulder around 490 nm (Fig. A2a). Unlike what happens with the previous fluorophore, in this case no changes in the shape of the spectrum can be detected as a function of the solvent. Once again, emission intensity is higher in lower polarity solvents, and a significant bathochromic shift of λ_{max} occurs on increasing solvent polarity with $\Delta\lambda = 28$ nm on going from chloroform to water (Fig. A2b). Finally, for **Mor-NI-Im**, we found a behavior similar to the one of **Pyrr-NI-Im**. Once again, the emission spectrum changes shape as a function of the solvent, transitioning for a two-peak spectrum in the lower polar solvents (chloroform and DCM) to a bathochromically shifted single band in highly polar solvents, like water. Once again, emission intensity diminishes as the solvent polarity increases with a significant bathochromic shift of λ_{max}, with $\Delta\lambda = 16$ nm (Fig. A3b) [34, 35].

To obtain further information on the photophysical properties of the three NI-derivatives in solution, we determined their relative fluorescence quantum yield (Φ_F) in some of the solvents considered, by using a reported procedure [34]. Depending on the solvent or fluorophore, the standards used were 9,10-diphenylanthracene or sodium fluorescein [35]. The results obtained are reported in Table 1.

The results reported in Table 1 are in line with the solvent dependent fluorescence spectra, exhibiting a clear increase in quantum yield on decreasing solvent polarity. In general, the values of Φ_F of **Pyrr-NI-Im** and **Pyrr-NI-Glu** follow a similar trend, whereas **Mor-NI-Im** appears as the least emissive fluorophore. However, unlike **Pyrr-NI-Im** and **Pyrr-NI-Glu**, the values of Φ_F for **Mor-NI-Im**, show a slight increase on going from DMSO to water.

3.3. *Aggregation of the fluorophores in aqueous solution*

Summarizing, the results collected hint at the possibility of supramolecular aggregation of the three fluorophores in water. To obtain further information on this, we carried out UV–vis and fluorescence measurements on solutions containing a constant concentration of fluorophores, in water/DMSO mixtures, spanning the full compositional range. The UV–vis spectra relevant to **Pyrr-NI-Im** are shown in Fig. 5, while the other ones are reported in Fig. A4. In addition, all the values of λ_{max} as a function of solvent composition, are reported in Table A3.

Perusal of the plots reported in Fig. 4a, shows a regular shift of λ_{max}

Table 1
Relative quantum yields of the fluorophores in selected solvents.

Solvent	Φ_F Pyrr-NI-IM (%)	Φ_F Pyrr-NI-Glu (%)	Φ_F Mor-NI-IM (%)
Chloroform	90	100	58
Dichloromethane	65	66	37
Tetrahydrofuran	12	19	23
DMSO	10	4	1
H_2O/DMSO 80:20 (v:v)	4	1	2
H_2O	2	1	5

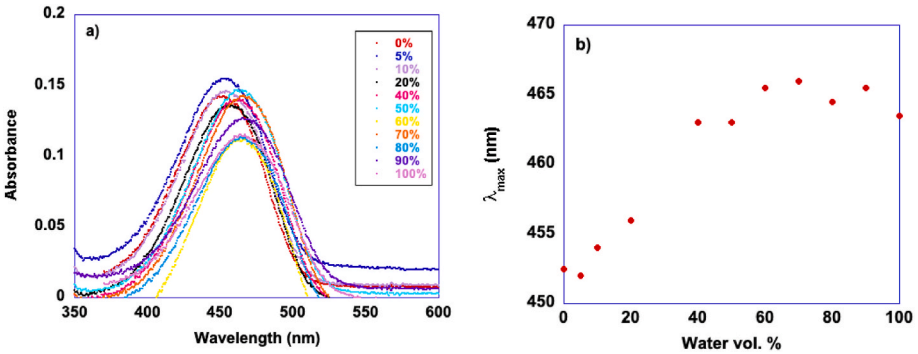

Fig. 5. a) Superimposed Uv–vis spectra of **Pyrr-NI-Im** ($5.5 \cdot 10^{-6}$ M) in water/DMSO mixtures of different composition and b) plot of λ_{max} as a function of solvent relative water amount in the mixtures.

towards longer wavelength as the amount of water increases. In particular, as shown in Fig. 5b, λ_{max} increases until reaching a plateau value at 60 vol %, with a bathochromic shift of 15 nm. A closely similar trend of both spectra and λ_{max} can be observed for **Pyrr-NI-Glu** (Figs. A4a–b), with a plateau composition of 60 vol% of water and a redshift of 17 nm. This bathochromic shift on increasing water content, can suggest the formation of *J*-aggregates [24,49]. Conversely, **Mor--NI-Im** exhibits a different behavior (Figs. A4c–d). In this case, the variation of λ_{max} as a function of solvent composition is lower, 8 nm, with a different trend. Upon increasing the amount of water, λ_{max} undergoes a redshift reaching a maximum value at 50 vol%, followed by a gradual blueshift (Fig. A4d).

We used the same approach for the fluorescence spectra in water/DMSO mixtures, obtaining the spectra reported in Fig. 6 for **Pyrr-NI-Im**, while the other ones are shown in Fig. A5. In addition, representative pictures of the sample solution are reported in Fig. 6c.

Looking at the spectra reported in Fig. 6a, clearly shows that, on increasing water content, emission λ_{max} undergoes redshift, from 535 nm to 548 nm, associated to a reduction in intensity. The trend of this latter, as a function of solvent composition, reported in Fig. 6b, shows a regular decrease, with a significant change in slope at a composition of 50 vol %. This can be interpreted as a transition from the molecularly dissolved state to a mainly aggregated state at this composition. Similar conclusions can be drawn for the other fluorophores.

As already said, all the results so far collected hint at the occurrence of supramolecular aggregation in aqueous solution, for all the three fluorophores. Consequently, we set out to obtain quantitative and mechanistic information on the self-assembly process by concentration- and temperature dependent spectroscopic investigations. However, this requires the use of high concentrations of fluorophores. Since in the case

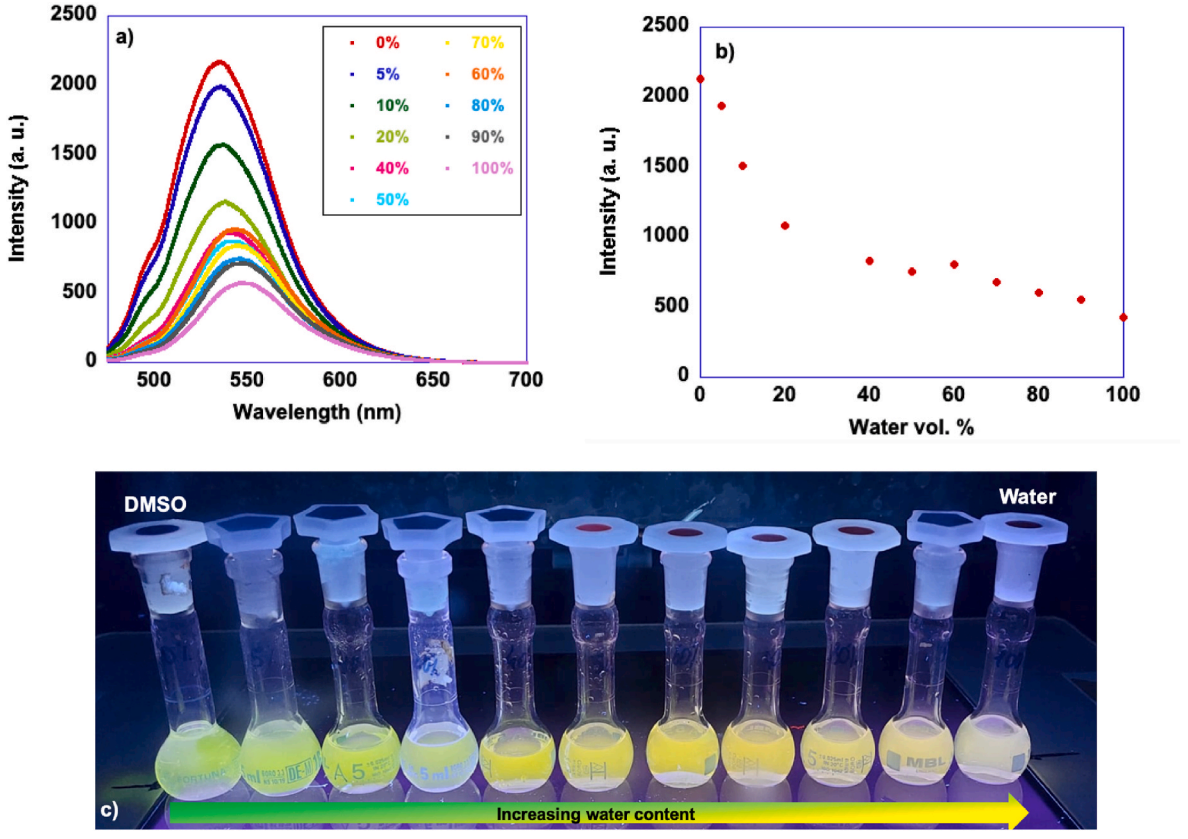

Fig. 6. a) Superimposed fluorescence spectra of **Pyrr-NI-Im** ($5.5 \cdot 10^{-6}$ M) in water/DMSO mixtures of different composition, b) plot of intensity a function of solvent relative water amount in the mixtures and c) representative picture of the sample solutions.

of Pyrr-NI-Im we encountered some solubility problems on increasing the concentrations, we chose to conduct the self-assembly study in water/DMSO 80 vol%. For **Pyrr-NI-Glu** and **Mor-NI-Im**, which did not show solubility issues, we conducted the investigation both in water and water/DMSO 80 vol%.

3.4. Self-assembly: concentration dependent investigation

Firstly, we carried out concentration dependent UV–vis measurements. The spectra obtained for **Pyrr-NI-Im in** water/DMSO 80 vol% are reported in Fig. 7a, while the spectra obtained for the other fluorophores are shown in Fig. A6.

The spectra reported in Fig. 7a and the plot λ_{max} as a function of concentration, clearly show a redshift in the absorption band, which amounts to 10 nm as the concentration of **Pyrr-NI-Im** increases. This indicates the formation of *J*-aggregates, reported in the literature also for other NI-derivatives [24,50].

Since such bathochromic shift is observed by increasing the concentration of fluorophore, keeping the solvent constant, this suggest that the shift results from *J*-aggregation and it is not induced by polarity changes.

Similar conclusions can be drawn for **Pyrr-NI-Glu,** by examining the plots reported in Figs. A6a–b. In this case, the increase in concentration leads to smaller but consistent shift at longer wavelengths, equal to 3 nm. For **Mor-NI-Im**, the trends of the spectra and of λ_{max}, reported in the plots of Figs. A6c–d, closely resemble the ones found for the other fluorophores in the same solvent medium, with a shift of λ_{max} equal to 2 nm, once again consistent with the formation of *J*-aggregates.

As reported in the literature [51], further evidence for the occurrence of aggregation in solution can be inferred by the non-linear trend of the extinction coefficient as a function of concentration. In Figs. A6e–f we report the plot of ε as a function of concentration for **Pyrr-NI-Glu** and **Mor-NI-Im**, which show a significant increase in the concentration range explored.

Conversely, a different picture emerges from the measurements carried out in water solution for **Pyrr-NI-Glu** and **Mor-NI-Im** (Fig. A7). In particular, the spectra of **Pyrr-NI-Glu** show no obvious shift in λ_{max} as a function of concentration (Figs. A7a–b), whereas in the case of **Mor-NI-Im**, the plot reported in Fig. A7d shows a significant blueshift (8 nm) of λ_{max} as a function of concentration, suggesting the formation of *H*-aggregates, evidencing a prominent effect of the solvent on the aggregation of this fluorophore, given that, as previously shown, upon adding 20 vol% of DMSO, *J*-aggregation occurs. Finally, the plots of the extinction coefficient as a function of concentration once again are consistent with the occurrence of aggregation in water, in both cases (Figs. A7e–f).

Next, to obtain quantitative and mechanistic information on the aggregation pathway, we carried out concentration-dependent fluorescence measurements. The spectra relevant to **Pyrr-NI-Im** are reported in Fig. 8, while the ones relevant to the other fluorophores are reported in Fig. A8. In addition, in Fig. 8b we report a representative picture of the sample solutions, irradiated under UV light.

The plot reported in Fig. 8a and the picture reported in Fig. 8b show that emission intensity increases with concentration and therefore with the formation of aggregates, which rules out the occurrence of aggregation caused quenching (ACQ). From the intensity values measured at each concentration, we determined the aggregation degree, α_{agg}, i.e the fraction of molecules present in solution in the aggregated form, by means of eq. (3)

$$\alpha_{agg} = \frac{[(I_C/C) - (I_{mon}/C_m)]}{[(I_{agg}/C_M) - (I_{mon}/C_m)]} \quad (3)$$

where C is the total concentration, I(C) is the emission intensity at a given C, I_{mon} is the emission intensity detected at the lowest concentration (C_m), which is assumed to be representative of the monomer, and I_{agg} is the emission intensity measured at the highest concentration (C_M) which is in turn assumed to be representative of the aggregates [52].

The plot of α_{agg} as a function of concentration, reported in Fig. 8c, displayed a trend consistent with the isodesmic model of supramolecular aggregation [53].

Then, non-linear fit of the curve, by means of equation (4), based on this aggregation pathway [54], allowed us to determine the equilibrium formation constants, K_{agg}, reported in Table 2.

$$\alpha_{agg} = 1 - \frac{2K_{agg}C + 1 - (4K_{agg}C + 1)^{0.5}}{2(K_{agg}C)^2} \quad (4)$$

The same investigation was carried out with the other fluorophores, obtaining the plots reported in Figure A8-9 and the constants reported in Table 2.

Examining K_{agg} values, points out that in the water/DMSO mixture, the trend of stability of the aggregates increases along the order **Pyrr-NI-Im** < **Mor-NI-Im** < **Pyrr-NI-Glu**, whereas, in water an opposite trend is found with **Pyrr-NI-Glu** < **Mor-NI-Im**. This can be explained by considering that in this case the stability of the aggregates is mainly driven by hydrophobic interactions, which are maximized for **Mor NI-Im**, which possesses a higher π-extension compared with **Pyrr-NI-Glu**.

In water/DMSO, the aggregation constants for **Pyrr-NI-Glu** is higher than the one of **Pyrr-NI-Im**, suggesting that, in this solvent, the higher ability of the former to establish hydrogen bonding enhances the stability of the aggregates. On the other hand, the higher aggregation constant found for **Mor-NI-Im**, compared with **Pyrr-NI-Im**, hints at a favorable effect of a higher dipole moment.

Comparing the aggregation constants for **Pyrr-NI-Glu** in water and water/DMSO solution, we find a higher value in the former case, consistent with the higher importance of hydrogen bonds upon adding DMSO. Accordingly, no significant difference in aggregation constant emerges for **Mor-NI-Im**, devoid of hydrogen bond donor sites, upon changing solvent. Finally, we can evaluate the effect of changing the substituent in the aromatic core from a halogen to a secondary amine group by comparing the aggregation constant in water of **Pyrr-NI-Glu**

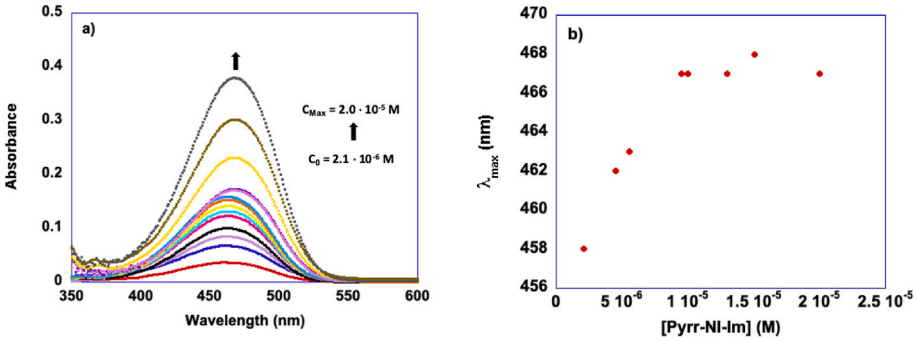

Fig. 7. a) Superimposed UV–vis spectra of **Pyrr-NI-Im** in water/DMSO 80 vol% at variable concentration and b) plot of λ_{max} as a function of concentration.

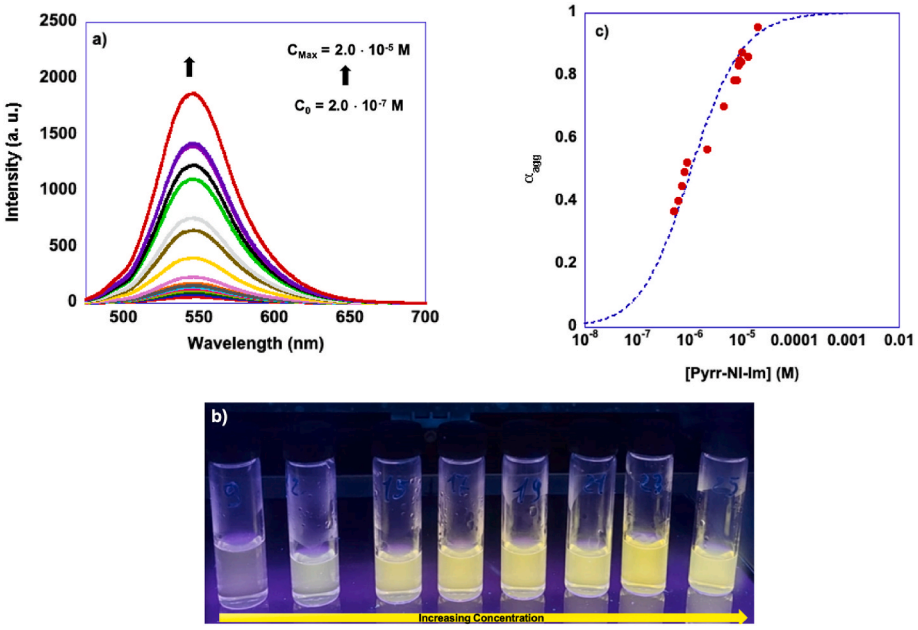

Fig. 8. a) Superimposed fluorescence spectra of **Pyrr-NI-Im** in water/DMSO 80 vol% at variable concentration, b) representative picture of sample solutions irradiated under UV light and c) plot of aggregation degree as a function of concentration.

Table 2
Values of K_{agg} obtained.

Fluorophore	Solvent	K_{agg} (M^{-1})
Pyrr-NI-Im	Water/DMSO 80 vol%	$(5.5 \pm 0.5)\cdot10^5$
Pyrr-NI-Glu	Water/DMSO 80 vol%	$(1.8 \pm 0.1)\cdot10^6$
Pyrr-NI-Glu	Water	$(5.0 \pm 0.4)\cdot10^5$
Mor-NI-Im	Water/DMSO 80 vol%	$(7.4 \pm 0.4)\cdot10^5$
Mor-NI-Im	Water	$(7.7 \pm 0.4)\cdot10^5$

with the one of a related compound only differing for the presence of a chlorine atom instead of the pyrrolidinyl group in the same position, determined in a previous work [25].

The aggregation constant is indeed higher in the case of **Pyrr-NI-Glu** ($K_{agg} = 5.0 \cdot 10^5$ M^{-1} and $3.0 \cdot 10^4$ M^{-1} for the chlorinated compound), consistent with the aforementioned favorable effect of hydrophobic interactions.

3.5. Self-assembly: temperature-dependent investigation

To obtain thermodynamic information about the aggregation process, we carried out temperature-dependent UV–vis spectra for all fluorophores. To this aim, we recorded the spectra at different temperatures of solutions containing a fixed concentration of fluorophore. This concentration was chosen so that the fluorophores are present in solution predominantly in the aggregated form. The spectra obtained in water/DMSO 80 vol%, reported in Figure A10a-c, show that only very slight variation in absorbance were obtained in the temperature range considered. This was also the case of the spectra of **Mor-NI-Im** in water, as a function of temperature, reported in Fig. A10d.

Differently, upon increasing the temperature, we observed a larger variation in absorbance for **Pyrr-NI-Glu**, reported in Fig. 9a.

The spectra reported in Fig. 9a show that, unlike what happens in water/DMSO 80 vol%., for **Pyrr-NI-Glu** in water, absorbances steadily increase on raising the temperature. From the value of absorbances at each temperature we were able to calculate the relevant values of α_{agg}, by means of Equation (5)

$$\alpha_{agg}(T) = \frac{(A_{(T)} - A_{mon})}{(A_{agg} - A_{mon})} \quad (5)$$

where $A_{(T)}$ is the absorbance of the solution at a given temperature, A_{mon} the absorbance measured at the highest temperature, which is assumed to be representative of the monomer, and A_{agg} is the absorbance measured at the lowest temperature, which in turn is assumed to be representative of the aggregate. Then, we plotted α_{agg} as a function of temperature and fitted the plot (Fig. 9b) by means of equation (6), based on the isodesmic model,

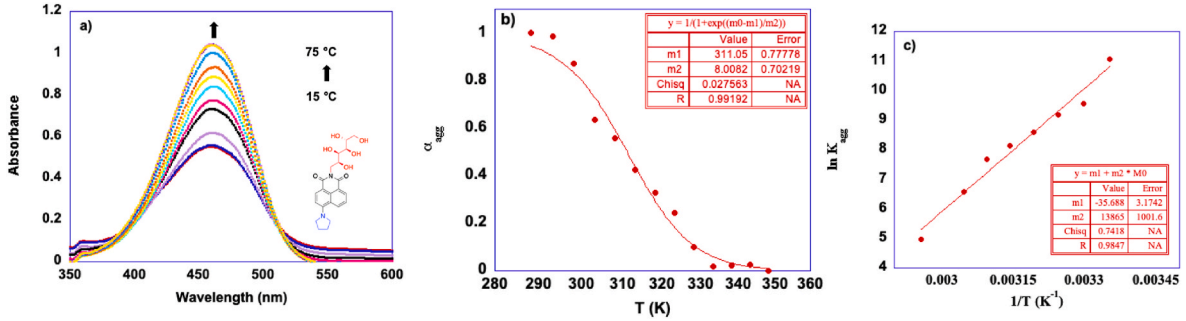

Fig. 9. a) Superimposed UV–vis spectra of **Pyrr-NI-Glu** ($7.8 \cdot 10^{-5}$ M) in water at variable temperature, b) plot of α_{agg} as a function of temperature and c) van 't Hoff plot for **Pyrr-NI-Glu** in water.

$$\alpha_{agg}(T) = 1 - \frac{1}{1 + \exp\,(T - T_m/T^*)} \quad (6)$$

where T_m is the melting temperature of the aggregate, *i.e.* the temperature at which α_{agg} is 0.5, while T* is a characteristic temperature related to the slope of the curve at T_m [55].

These data allowed us to determine K_{agg} at each temperature. Details of this calculation have been reported elsewhere [55,56]. Then, we applied a van 't Hoff treatment to determine the thermodynamic parameters associated to the aggregation process. This treatment could be applied to all cases, with the only exception of **Mor-NI-Im** in water, because the variation of absorbance was too low to extract thermodynamic parameters. The plot obtained for **Pyrr-NI-Glu** in water is reported in Fig. 9c, while the ones relevant to all fluorophores in water/DMSO 80 vol% are reported in Fig. A11. The values of the variations of enthalpy (ΔH_{agg}) and entropy (ΔS_{agg}) obtained, together with the melting temperatures of the aggregates, are reported in Table 3.

Examination of the values of T_m reported in Table 3 shows that the values in water/DMSO 80 vol% are practically comparable in all cases, whereas the lowest value was found for **Pyrr-NI-Glu** in water. Moving to the thermodynamic parameters, in general they are consistent with an enthalpy-driven association process. The lowest value of $\Delta S_{agg,}$ obtained in the case of **Pyrr-NI-Glu** in water, points out that these aggregates are the most organized ones. The largest enthalpy variation was also found for this system.

In general, in water/DMSO solution, the thermodynamic parameters appear barely affected by the substitution of the core and imide positions. The larger change in magnitude was found for the thermodynamic parameters relevant to **Pyrr-NI-Glu**, which diminish on going from water/DMSO to water solution. In particular, the reduction in ΔH_{agg} is consistent with solvation effects weakening hydrogen bonds on going to purely aqueous solution.

3.6. Morphology of the aggregates

To obtain information on the morphology of the aggregates, we recorded SEM images of samples prepared by drop-casting on aluminium stub solution of the fluorophores, at a suitable concentration at which the fluorophore are mainly present in the aggregated form. To have a meaningful comparison, we recorded images of samples obtained from solutions in the same solvent, water/DMSO 80 vol%. The images acquired are reported in Fig. 10 and A12.

The images reported in Fig. 10 clearly show that the aggregates of **Pyrr-NI-Im** have a distinct morphology compared with the other ones, as they are constituted by large, uniformly dispersed, irregular-shaped objects. Conversely, the aggregates of both **Pyrr-NI-Glu** and **Mor-NI-Im**, show a sponge-like morphology, featured by spheroidal structures.

3.7. Solid state fluorescence spectra

Finally, to gain information on the emission ability of our fluorophores in the solid state, we recorded emission spectra of thin films obtained by solutions of the fluorophores characterized by a prominent presence of aggregates. The spectra obtained, superimposed to the one of the parent solutions, are reported in Fig. 11.

The spectra reported for **Pyrr-NI-Glu** and **Mor-NI-Im** in Fig. 11, clearly show that on going from solution to solid state, in all cases, λ_{max} shifts to much shorter wavelengths and intensity significantly increases, pointing at the formation of emissive aggregates in the solid state. It is worth noting that this happens also for **Pyrr-NI-Im**, in which case the emission intensity was so high, that exceeded instrumental limits when recorded under the same operative conditions of the solution state. In Fig. A13, we report the superimposed spectra for **Pyrr-NI-Im**, in which case, the solid-state spectra was obtained at a lower instrumental sensitivity compared with the one in solution, with the sole aim to show the position of the emission peak. Notably, in the case of **Pyrr-NI-Glu**, core substitution with pyrrolidyl moiety induced the obtainment of emissive aggregates in the condensed phase, given that a closely related fluorophore, with chloride atom in the 4-position of the NI-ring was found non-fluorescent in the solid state [25].

Table 3
Values of T_m and of thermodynamic parameters associated to the aggregation process.

Fluorophore	Solvent	T_m (°C)	ΔH_{agg} (kJ/mol)	ΔS_{agg} (J/mol K)
Pyrr-NI-Im	Water/DMSO 80 vol%	45 ± 1	−73 ± 5	−155 ± 15
Pyrr-NI-Glu	Water/DMSO 80 vol%	44.9 ± 0.9	−69 ± 3	−145 ± 8
Pyrr-NI-Glu	Water	37.9 ± 0.8	−124 ± 1	−330 ± 40
Mor-NI-Im	Water/DMSO 80 vol%	43.2 ± 0.9	−70 ± 2	−149 ± 6

3.8. Fluorescent sensing of drugs in solution

Having studied and characterized the aggregates formed in solution by the fluorophore, we went on to assess the ability of these aggregates to function as sensory probes for the detection of drugs in solution. To this aim, we conducted fluorescence measurements of solutions containing fixed concentration of **Pyrr-NI-Im**, **Pyrr-NI-Glu**, **and Mor-NI-Im**, and increasing amounts of drugs. The measurements were carried out in solution of water/DMSO 80 vol% for **Pyrr-NI-Im** and **Mor-NI-Im**, and in water for **Pyrr-NI-Glu** because in the other cases, no significant variations in fluorescence intensity were detected. The drugs considered were nalidixic acid, ciprofloxacin, diclofenac sodium salt, carbamazepine and ketoprofen (Fig. 1). Preliminarily, we verified the absence of overlapping in the adsorption spectra of the drugs with those of the probe, to ensure that at the λ_{exc} used for the spectra, the emission is solely due to the fluorophores. As can be inferred by the superimposed adsorption spectra reported in Fig. A14, there is no such superposition. For the sake of clarity, we will discuss the sensing experiments with each fluorophore, separately in the following sections.

Sensing measurements with **Pyrr-NI-Im** were carried out in water/DMSO 80 vol%, at a concentration of fluorophore of $1.0 \cdot 10^{-5}$ M, in the presence of drugs in the concentration range $1.0 \cdot 10^{-7}$ M ÷ $9.0 \cdot 10^{-5}$ M. The plots of spectra and emission intensity as a function of concentration relevant to the measurements in the presence of ketoprofen are reported in Fig. 12, while those obtained in the presence of the other drugs are reported in Figures A15-18.

In all cases, increasing the concentration of drugs induces a quenching of emission, until reaching a plateau value. For all the plots, we identified the linear response range. Fitting of this region allowed us to determine the Limit of Detection (LOD), and the Limit of Quantification, according to a procedure reported in the literature (see experimental section for details) [36]. The values of LOD and LOQ obtained are reported in Fig. 13 and in Table A5.

Results reported in Fig. 13a show that **Pyrr-NI-Im** is sensitive to the presence of all the drugs considered, with LOD values falling within the micromolar range. LOD and LOQ values increase along the order ketoprofen < ciprofloxacin < carbamazepine < nalidixic acid ≈ diclofenac. Comparing the trend observed with the structures of the drugs considered, suggests that the sensitivity of the probe is negatively affected by an increase in molecular rigidity, and by the presence of a negatively charged moieties, like the carboxylate anion in diclofenac.

The same approach was applied to assess the sensing ability of the two other probes, **Mor-NI-Im** and **Pyrr-NI-Glu.** The results obtained are reported in Figs. 13b–14, A19-22 and Table A6.

It is important to note that the behavior of **Mor-NI-Im** and **Pyrr-NI-Glu** is substantially different from the one of **Pyrr-NI-Im.** More specifically, **Mor-NI-Im** showed appreciable emission variations only in water/DMSO 80 vol%, in the presence of ciprofloxacin and ketoprofen.

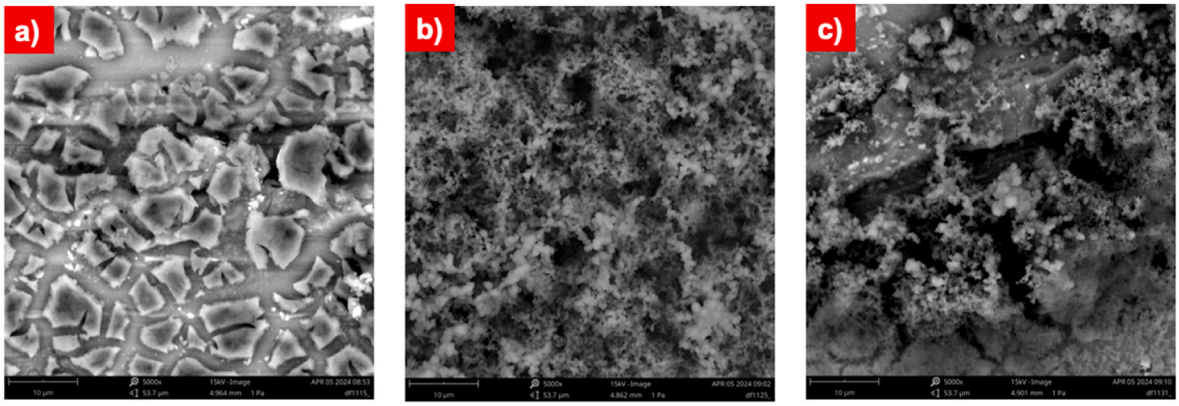

Fig. 10. SEM images of aggregates formed by solution in water/DMSO 80 vol% of a) **Pyrr-NI-Im** ($1.0 \cdot 10^{-5}$ M), b) **Pyrr-NI-Glu** ($2.5 \cdot 10^{-5}$ M), and c) **Mor-NI-Im** ($2.5 \cdot 10^{-5}$ M), at 5000× magnification.

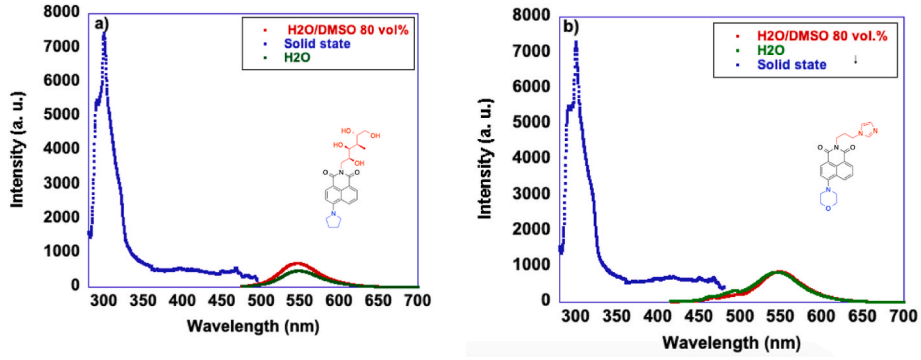

Fig. 11. Superimposed fluorescence solid-state and solution spectra of a) **Pyrr-NI-Glu** ($2.5 \cdot 10^{-5}$ M in water/DMSO 80 vol% and water), and b) **Mor-NI-Im** ($2.5 \cdot 10^{-5}$ M in water/DMSO 80 vol% and water).

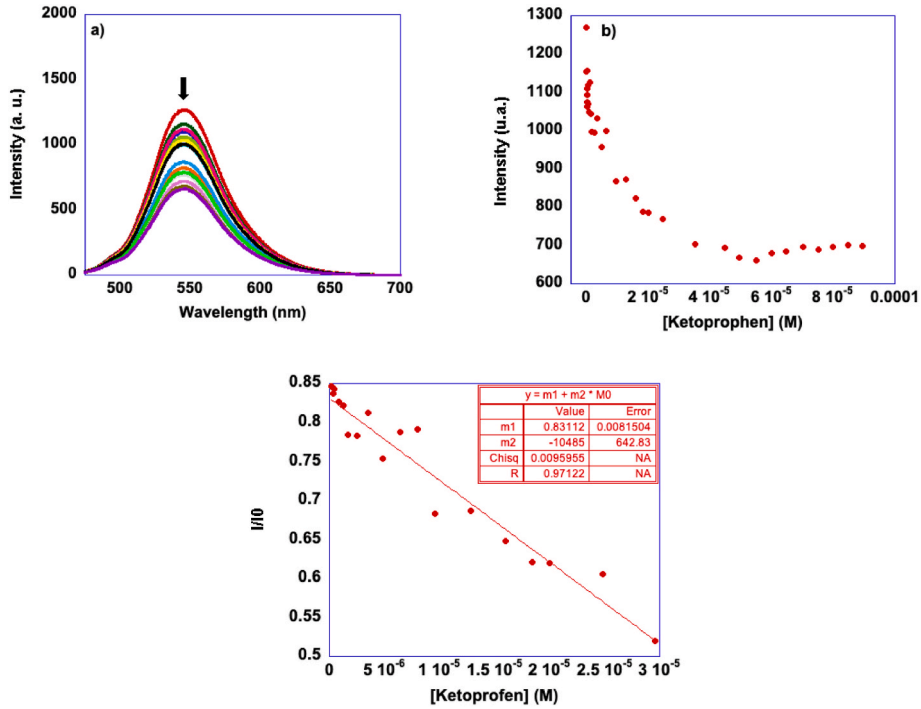

Fig. 12. a) Superimposed fluorescence spectra for solutions of **Pyrr-NI-Im** ($1.0 \cdot 10^{-5}$ M) in water/DMSO 80 vol% in the presence of increasing concentrations of ketoprofen, b) plot of fluorescence intensity as a function of drug concentration and c) plot of quenching ratio as a function of drug concentration, within the linear response range.

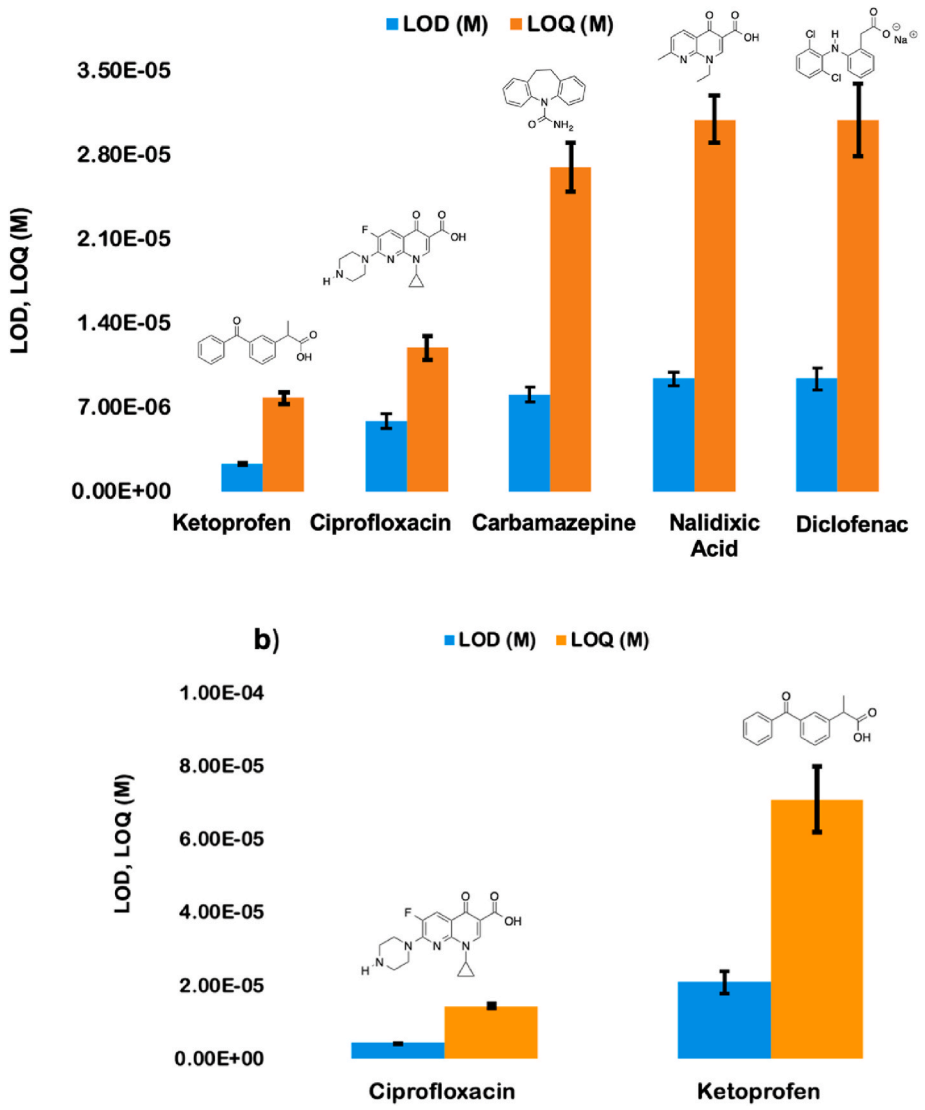

Fig. 13. Values of LOD and LOQ for a) **Pyrr-NI-Im** ($1.0 \cdot 10^{-5}$ M) and b) **Mor-NI-Im** ($2.5 \cdot 10^{-5}$ M) in water/DMSO 80 vol%, in the presence different drugs.

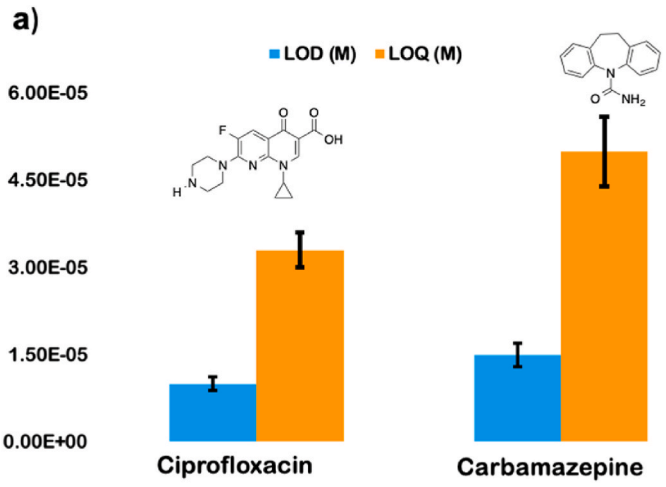

Fig. 14. Values of LOD and LOQ for **Pyrr-NI-Glu** ($1.0 \cdot 10^{-5}$ M) in water.

However, the emission of **Mor-NI-Im**, was less sensitive to the presence of drugs, compared to **Pyrr-NI-Im**.

In addition, upon increasing the amount of drugs, after an initial quenching, the emission showed a regular increase. On the other hand, **Pyrr-NI-Glu** displayed significant in emission intensity only in water, and in the presence of ciprofloxacin and carbamazepine. Thus, these two probes were less sensitive but also more selective, compared with **Pyrr-NI-Im**.

Values of LOD and LOQ (Table A6) are significantly higher than the ones detected for **Pyrr-NI-Im**. However, given the low number of drugs considered, in this case it is difficult to pinpoint what parameter favors the detection of the drugs.

It is important to further compare the performance of two probes in the same solvent, namely **Pyrr-NI-Im** and **Mor-NI-Im** in water/DMSO 80 vol%. In particular, comparing the LOD and LOQ values reported in Tables A5-6, we can observe that **Pyrr-NI-Im** outperforms **Mor-NI-Im** in the presence of ketoprofen, whereas their performance is comparable in the presence of ciprofloxacin.

Regarding the sensing mechanism, in all cases we obtained non-linear intensity quenching- or enhancement plots, which as reported in the literature, suggest the occurrence of more than one mechanism operating [57]. However, based on the absence of overlapping between the emission spectra of the probes and the absorption spectra of the

drugs, we can rule out inner filter effects [58]. We can as well rule out the formation of ground-state complexes, since no change in the absorption spectra of the probes was detected in the presence of the drugs considered.

To better investigate the possible sensing mechanism, we recorded the fluorescence spectra of the probes as a function of pH. It is indeed reported in the literature that the dependence of the emission intensity from pH can shed light on the possible occurrence of photoinduced electron transfer (PET) [59–61]. The results obtained are reported in Fig. 15.

Examination of the plots reported in Fig. 15, shows a very different behavior among the probes, as a function of pH. In particular, for the two imidazole-functionalized probes, **Pyrr-NI-Im** and **Mor-NI-Im,** fluorescence intensity significantly increases on upon lowering the pH (Fig. 15a and c), which suggests the suppression of PET by protonation of the piperidino- and morpholino moieties, as reported in the literature for similar fluorophores [62]. Notably, we can hypothesize also a contribution of the imidazole group, since when this group is absent and replaced by D-glucamine, fluorescence is no longer affected by pH suggesting the absence of PET.

Based on all these observations we can hypothesize that a possible mechanism for sensing by **Mor-NI-Im,** is the suppression of PET upon interaction with the drugs, as testified by the increase in intensity in the presence of higher concentrations of drugs. Conversely, the quenching of fluorescence detected for **Pyrr-NI-Im** in the presence of drugs, rules out the PET-based sensing but may be ascribed to the occurrence of intramolecular charge transfer (ICT), which is another process found in 4-amino-functionalized NI-derivatives [62]. Finally, for **Pyrr-NI-Glu**, the observed trend is quite complex, resulting from more the one concomitant mechanisms, which are difficult to dissect. The concomitant occurrence of different sensing mechanisms has previously been reported for NI-derivatives, for example simultaneous ICT and PET [63].

3.9. Incorporation of the probe onto solid supports

Having ascertained that the probes can in fact detect some drugs in solution, and that they are able to emit also in the solid state, we went on to explore the possibility of embedding them onto solid supports, like filter paper strips or polymer film. In particular, to explore this possibility, we chose to employ the most sensitive probe, namely **Pyrr-NI-Im**. In both cases, we embedded the probe onto the solid supports and immersed the resulting materials in an aqueous solution of the drug. Finally, we recorded the solid-state fluorescence spectrum to evaluate if the presence of the drug significantly influences the emission.

In the case of the filter paper strip, we first soaked a square filter paper strip (2 cm × 2 cm) in a solution of **Pyrr-NI-Im** ($1{\cdot}10^{-5}$ M) in dichloromethane and, after drying at room temperature, recorded the solid-state emission spectrum. Then, we immersed similar **Pyrr-NI-Im**-laden filter paper strips in aqueous solutions of ketoprofen of different concentrations, $4.80{\cdot}10^{-6}$ M and $1.29{\cdot}10^{-5}$ M, for 5 min and then dried at room temperature. The solid-state emission spectra of these filter paper strips are reported in Fig. 16a.

The spectra reported in Fig. 16a show a significant quenching of emission upon increasing the concentration of drug, therefore suggesting potential for the obtainment of a solid-supported sensor. A similar approach was followed to support **Pyrr-NI-Im** as a sensory probe on a poly(3-hydroxybutirate) (PHB) film. In this case, the film was prepared by solvent casting from chloroform solution, in the presence of the amount of **Pyrr-NI-Im** yielding a concentration in solution of $1{\cdot}10^{-5}$ M. We recorded the solid-state emission spectrum of a rectangular section of film before and after being soaked in a solution of ketoprofen $2.5{\cdot}10^{-5}$ M and dried at room temperature. The spectra obtained, reported in Fig. 16b, once again reveal a significant quenching in the presence of the drug. In summary, **Pyrr-NI-Im** is a sensitive probe for fluorescent sensing of drugs in aqueous solutions, but also shows potential to be embedded onto solid supports.

Finally, to assess the performance of our system we report below Table 4, comparing our best results, with recent literature examples, dealing with fluorescent sensing of the ketoprofen in aqueous solutions. We chose to limit our comparison to the detection of ketoprofen, because it showed the lowest LOD with **Pyrr-NI-Im**.

Perusal of the results reported in Table 4 shows that our system has a comparable performance with the one based on modified CdTe quantum dots reported by Molina Garcia et al. (entry 1 and 2) [64].

Conversely, the performance of our system was inferior to the ones of anthracenyl-functionalized polyamine receptors reported by Bencini et al. in H_2O/EtOH solution [65], and to the one reported by Chandel [66], employing N-doped carbon dots encapsulated in mesoporous silica (entries 1,3–4).

Finally, all these systems are outperformed by the one described by Bhogal [67], based on surface molecularly imprinted carbon dots, which achieves the lowest LOD reported for the fluorescent sensing of ketoprofen in aqueous solutions.

It is worth noting, that our system is the only one reported in Table 4, based on supramolecular aggregates. There are indeed few works reported for the sensing of drugs by supramolecular aggregates but they are used for the sensing of drugs different from those investigated here, mostly focused on heparin [68–70].

4. Conclusions

In this work, we prepared three novel 1,8-napthylimide derivatives, **Pyrr-NI-Im**, **Pyrr-NI-Glu** and **Mor-NI-Im**, functionalized with cyclic amine groups at the core position and bearing an imidazole or D-glucamine group at the imide position. We studied the photophysical properties and the self-assembling ability of these NI-derivatives, finding that they form supramolecular aggregates in water and water/DMSO solutions. With the exception of **Mor-NI-Im** in water, *J*-aggregates were formed by all derivatives, following an isodesmic aggregation pathway. In addition, we found that **Pyrr-NI-Glu** forms the most stable aggregates

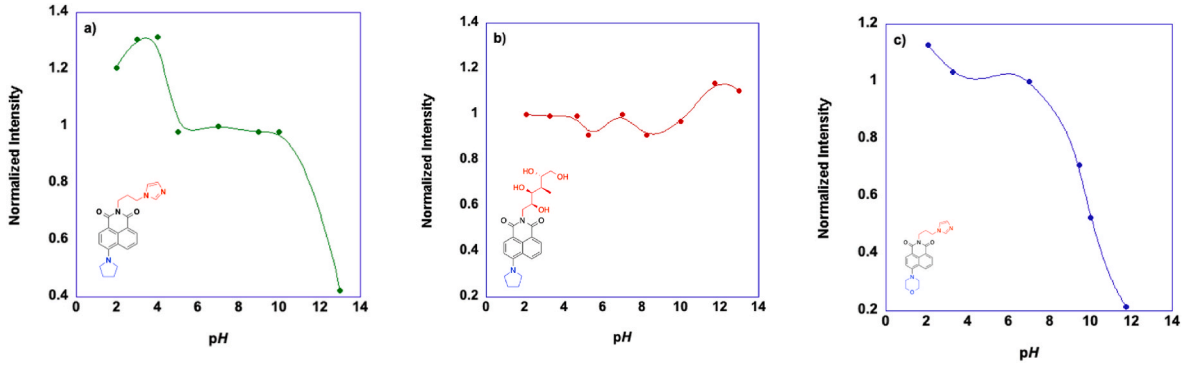

Fig. 15. Plots of normalized fluorescence intensity for a) **Pyrr-NI-Im** ($2.5 \cdot 10^{-4}$ M), b) **Pyrr-NI-Glu** ($1.0 \cdot 10^{-5}$ M) and c) **Mor-NI-Im** ($1.0 \cdot 10^{-5}$ M) in water.

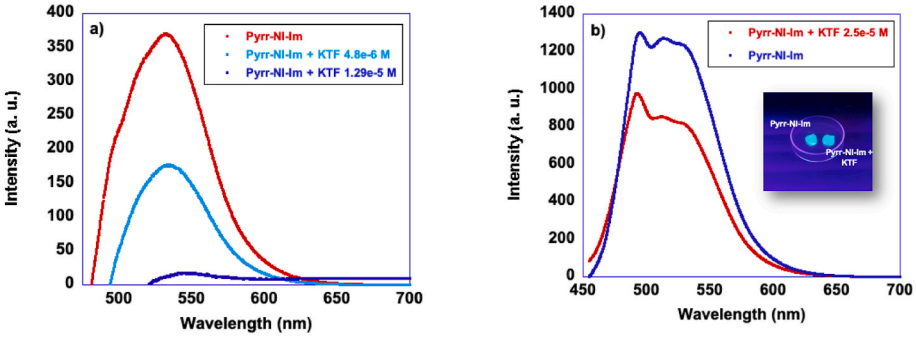

Fig. 16. Solid-state emission spectra of a) filter paper strips laden with **Pyrr-NI-Im** and then in solutions of ketoprofen and b) PHB-film laden with **Pyrr-NI-Im** and then soaked in a solution of ketoprofen, inset shows picture under UV-light of the probe-laden film and the same film after soaking in ketoprofen solution.

Table 4
Comparison of LOD of **Pyrr-NI-Im** and literature systems for sensing of ketoprofen in aqueous solutions.

Entry	Sensor	LOD (μM)
1	**Pyrr-NI-Im**[a]	(2.3 ± 0.1)
2	Quantum dots [64]	2.3
3	Polyamine receptors [65]	0.25
4	N-doped carbon dots [66]	<0.3
5	Hybrid carbon dots [67]	0.01

[a] This work.

in water/DMSO 80 vol%, whereas in water the most stable aggregates are formed by **Mor-NI-Im**. We also obtained information on the thermodynamic parameters associated with the self-assembly process, in all cases consistent with an enthalpy-driven association process. Notably, the aggregates maintained their emission also in the solid state.

Subsequently, we investigated the possibility of using such supramolecular aggregates as fluorescent sensory probes for the detection in aqueous solutions of drugs belonging to different classes. We found that the most sensitive probe is **Pyrr-NI-Im**, whose emission underwent quenching in the presence of all the drugs considered, with the highest sensitivity towards ketoprofen with LOD of (2.3 ± 0.1) μM and LOQ of (6.9 ± 0.3) μM. Conversely, the emission of **Pyrr-NI-Glu** and **Mor-NI-Im** was less sensitive to the presence of drugs in solutions, exhibiting higher sensitivity towards ciprofloxacin, with LOD and LOQ values one order of magnitude higher than those obtained for **Pyrr-NI-Im**. It is important to note that in general, the probes used simply establish the presence the presence of the drugs in the sample, but are not selective to each drug.

Finally, we evaluated the possibility of embedding the best-performing probe onto solid supports like filter paper strips or poly(3-hydroxybutirate) and if the emission of the ensuing solids is affected by the presence of a drug like ketoprofen in solution. After soaking the fluorophore-doped solid in solutions of ketoprofen at different concentrations, we found significant quenching of solid-state emission as a function of the concentration of drug.

CRediT authorship contribution statement

Salvatore Marullo: Writing – original draft, Visualization. **Eleonora Capuano:** Investigation. **Francesca D'Anna:** Writing – review & editing, Supervision, Funding acquisition, Conceptualization.

Declaration of competing interest

The authors declare that they have no known competing financial interests or personal relationships that could have appeared to influence the work reported in this paper.

Acknowledgements

We thank MUR for funding, SiciliAn MicronanOTecH Research And Innovation CEnter "SAMOTHRACE" (MUR, PNRR-M4C2, ECS_00000022), spoke 3 - Università degli Studi di Palermo "S2-COMMs - Micro and Nanotechnologies for Smart & Sustainable Communities"

The funding source had no role in analysis, design, interpretation of results and report writing.

SEM images were acquired at ATeN Center of University of Palermo—Laboratorio di Preparazione e Analisi di Biomateriali.

Appendix A. Supplementary data

Supplementary data to this article can be found online at https://doi.org/10.1016/j.dyepig.2025.112881.

Data availability

All data supporting this work are shared in Supporting Information

References

[1] Daughton CG. Non-regulated water contaminants: emerging research. Environ Impact Assess Rev 2004;24:711–32. https://doi.org/10.1016/j.eiar.2004.06.003.
[2] Daughton CG. Environmental stewardship and drugs as pollutants. Lancet 2002;360:1035–6. https://doi.org/10.1016/S0140-6736(02)11176-7.
[3] Rastogi A, Tiwari MK, Ghangrekar MM. A review on environmental occurrence, toxicity and microbial degradation of non-steroidal anti-inflammatory drugs (NSAIDs). J Environ Manag 2021;300:113694. https://doi.org/10.1016/j.jenvman.2021.113694.
[4] Santos LHMLM, Araújo AN, Fachini A, Pena A, Delerue-Matos C, Montenegro MCBSM. Ecotoxicological aspects related to the presence of pharmaceuticals in the aquatic environment. J Hazard Mater 2010;175:45–95. https://doi.org/10.1016/j.jhazmat.2009.10.100.
[5] Delli Compagni R, Polesel F, von Borries KJF, Zhang Z, Turolla A, Antonelli M, Vezzaro L. Modelling the fate of micropollutants in integrated urban wastewater systems: extending the applicability to pharmaceuticals. Water Res 2020;184:116097. https://doi.org/10.1016/j.watres.2020.116097.
[6] Siddiqui MR, AlOthman ZA, Rahman N. Analytical techniques in pharmaceutical analysis: a review. Arab J Chem 2017;10:S1409–21. https://doi.org/10.1016/j.arabjc.2013.04.016.
[7] Walekar L, Dutta T, Kumar P, Ok YS, Pawar S, Deep A, Kim K-H. Functionalized fluorescent nanomaterials for sensing pollutants in the environment: a critical review. TrAC, Trends Anal Chem 2017;97:458–67. https://doi.org/10.1016/j.trac.2017.10.012.
[8] Krämer J, Kang R, Grimm LM, De Cola L, Picchetti P, Biedermann F. Molecular probes, chemosensors, and nanosensors for optical detection of biorelevant molecules and ions in aqueous media and biofluids. Chem Rev 2022;122:3459–636. https://doi.org/10.1021/acs.chemrev.1c00746.
[9] Wu D, Sedgwick AC, Gunnlaugsson T, Akkaya EU, Yoon J, James TD. Fluorescent chemosensors: the past, present and future. Chem Soc Rev 2017;46:7105–23. https://doi.org/10.1039/C7CS00240H.
[10] Ghosh S, Rana A, Biswas S. Metal–organic framework-based fluorescent sensors for the detection of pharmaceutically active compounds. Chem Mater 2024;36:99–131. https://doi.org/10.1021/acs.chemmater.3c02459.
[11] Picchetti P, Balli MV, Baker S, Kumar NM, Gruhs P, Prodi L, Biedermann F. Unimolecular Cucurbit[7]uril-Based indicator displacement assay with dual signal-

readout for the detection of drugs. Anal Sens 2024;4. https://doi.org/10.1002/anse.202400025.
[12] Selinger AJ, Krämer J, Poarch E, Hore D, Biedermann F, Hof F. Mixed host co-assembled systems for broad-scope analyte sensing. Chem Sci 2024;15:12388–97. https://doi.org/10.1039/D4SC02788D.
[13] Picci G, Aragoni MC, Arca M, Caltagirone C, Formica M, Fusi V, Giorgi L, Ingargiola F, Lippolis V, Macedi E, Mancini L, Mummolo L, Prodi L. Fluorescent sensing of non-steroidal anti-inflammatory drugs naproxen and ketoprofen by dansylated squaramide-based receptors. Org Biomol Chem 2023;21:2968–75. https://doi.org/10.1039/D3OB00324H.
[14] Wang Q, Li Z, Tao D-D, Zhang Q, Zhang P, Guo D-P, Jiang Y-B. Supramolecular aggregates as sensory ensembles. Chem Commun 2016;52:12929–39. https://doi.org/10.1039/C6CC06075G.
[15] Dai D, Yang J, Yang Y. Supramolecular assemblies with aggregation-induced emission properties for sensing and detection. Chem Eur J 2022;28. https://doi.org/10.1002/chem.202103185.
[16] Yao H, Zhou Q, Kan X-T, Niu Y-B, Naeem M, Wei T-B, Lin Q, Zhang Y-M. A signal amplification strategy for ultrasensitive detecting H2PO4− using metal coordinated supramolecular gel. J Mol Liq 2021;321:114500. https://doi.org/10.1016/j.molliq.2020.114500.
[17] Yuan L, Li M, Li J, Zhu T-F, Dong M, Liu L. Aggregation-induced signal amplification strategy based on peptide self-assembly for ultrasensitive electrochemical detection of melanoma biomarker. Anal Chim Acta 2024;1289:342214. https://doi.org/10.1016/j.aca.2024.342214.
[18] Moharana P, Santosh G. Amphiphilic perylene diimide-based fluorescent hemispherical aggregates as probes for metal ions. Spectrochim Acta 2023;297:122696. https://doi.org/10.1016/j.saa.2023.122696.
[19] Wu Y, Zhang Q, Zhao Y, Zhuang K, Fan Y, Zhang S, Zhang X, Huang K, Yao Z. A sensitive and selective fluorescent sensor for berberine chloride based on the supramolecular self-assembly of perylene diimide in aqueous solution. ACS Sustainable Chem Eng 2020;8:6517–23. https://doi.org/10.1021/acssuschemeng.0c01177.
[20] Gopikrishna P, Meher N, Iyer PK. Functional 1,8-Naphthalimide AIE/AIEEgens: recent advances and prospects. ACS Appl Mater Interfaces 2018;10:12081–111. https://doi.org/10.1021/acsami.7b14473.
[21] Wang Q, Wu H, Gao A, Ge X, Chang X, Cao X. Bis-naphthalimide-based supramolecular self-assembly system for selective and colorimetric detection of oxalyl chloride and phosgene in solution and gas phase. Chin Chem Lett 2023;34:107644. https://doi.org/10.1016/j.cclet.2022.06.067.
[22] Cao X, Zhao N, Gao A, Ding Q, Li Y, Chang X. Terminal molecular isomer-effect on supramolecular self-assembly system based on naphthalimide derivative and its sensing application for Mercury(II) and Iron(III) ions. Langmuir 2018;34:7404–15. https://doi.org/10.1021/acs.langmuir.8b00991.
[23] Cao X, Gao A, Hou J, Yi T. Fluorescent supramolecular self-assembly gels and their application as sensors: a review. Coord Chem Rev 2021;434:213792. https://doi.org/10.1016/j.ccr.2021.213792.
[24] Rizzo C, Cancemi P, Mattiello L, Marullo S, D'Anna F. Naphthalimide imidazolium-based supramolecular hydrogels as bioimaging and theranostic soft materials. ACS Appl Mater Interfaces 2020;12:48442–57. https://doi.org/10.1021/acsami.0c17149.
[25] Marullo S, Arena R, Lazzara G, Cavallaro G, Cacioppo M, D'Anna F. Fast and efficient sensing of drugs in water using self-assembling d-glucamine functionalized naphthalenediimide and 1,8-Naphthalimide fluorophores. Chem Eur J 2024. https://doi.org/10.1002/chem.202401944.
[26] Lin H-H, Chan Y-C, Chen J-W, Chang C-C. Aggregation-induced emission enhancement characteristics of naphthalimide derivatives and their applications in cell imaging. J Mater Chem 2011;21:3170. https://doi.org/10.1039/c0jm02942d.
[27] Alexiou MS, Tychopoulos V, Ghorbanian S, Tyman JHP, Brown RG, Brittain PI. The UV–visible absorption and fluorescence of some substituted 1,8-naphthalimides and naphthalic anhydrides. J. Chem. Soc., Perkin Trans. 1990;2:837–42. https://doi.org/10.1039/P29900000837.
[28] Thomas D, Rubio V, Iragavarapu V, Guzman E, Pelletier OB, Alamgir S, Zhang Q, Stawikowski MJ. Solvatochromic and pH-Sensitive fluorescent membrane probes for imaging of live cells. ACS Chem Neurosci 2021;12:719–34. https://doi.org/10.1021/acschemneuro.0c00732.
[29] Peters A. Amino derivatives of 1,8-naphthalic anhydride and derived dyes for synthetic-polymer fibres. Dyes Pigments 1985;6:349–75. https://doi.org/10.1016/0143-7208(85)85005-1.
[30] Grepioni F, d'Agostino S, Braga D, Bertocco A, Catalano L, Ventura B. Fluorescent crystals and co-crystals of 1,8-naphthalimide derivatives: synthesis, structure determination and photophysical characterization. J Mater Chem C 2015;3:9425–34. https://doi.org/10.1039/C5TC01518A.
[31] Ikawa Y, Ogawa H, Harada H, Furuta H. N-confused porphyrin possessing glucamine-appendants: aggregation and acid/base properties in aqueous media. Bioorg Med Chem Lett 2008;18:6394–7. https://doi.org/10.1016/j.bmcl.2008.10.079.
[32] Ohsedo Y, Oono M, Saruhashi K, Watanabe H. N-Alkylamido- <scp>d</scp> -glucamine-based gelators for the generation of thixotropic gels. RSC Adv 2014;4:48554–8. https://doi.org/10.1039/C4RA08346F.
[33] Nath JK, Baruah JB. Solvatoemissive dual fluorescence of N-(pyridylmethyl)-3-nitro-1,8-naphthalimides. J Fluoresc 2014;24:649–55. https://doi.org/10.1007/s10895-014-1353-8.
[34] Würth C, Grabolle M, Pauli J, Spieles M, Resch-Genger U. Relative and absolute determination of fluorescence quantum yields of transparent samples. Nat Protoc 2013;8:1535–50. https://doi.org/10.1038/nprot.2013.087.
[35] Brouwer AM. Standards for photoluminescence quantum yield measurements in solution (IUPAC technical report). Pure Appl Chem 2011;83:2213–28. https://doi.org/10.1351/PAC-REP-10-09-31.
[36] Miller JN. Basic statistical methods for analytical chemistry. Part 2. Calibration and regression methods. A review. Analyst 1991;116:3. https://doi.org/10.1039/an9911600003.
[37] Tansil NC, Xie H, Xie F, Gao Z. Direct detection of DNA with an electrocatalytic threading intercalator. Anal Chem 2005;77:126–34. https://doi.org/10.1021/ac0493469.
[38] Hao P, Xu Y, Shen J, Fu Y. Effect of positional isomerism on electron-transfer photochromism and photoluminescence of two pyromellitic diimide-based organic molecules. Dyes Pigments 2021;186:108941. https://doi.org/10.1016/j.dyepig.2020.108941.
[39] Billeci F, D'Anna F, Marullo S, Noto R. Self-assembly of fluorescent diimidazolium salts: tailor properties of the aggregates changing alkyl chain features. RSC Adv 2016;6. https://doi.org/10.1039/c6ra10250f.
[40] Ozdemir S, Varlikli C, Oner I, Ocakoglu K, Icli S. The synthesis of 1,8-naphthalimide groups containing imidazolium salts/ionic liquids using I−, PF6−, TFSI− anions and their photophysical, electrochemical and thermal properties. Dyes Pigments 2010;86:206–16. https://doi.org/10.1016/j.dyepig.2010.01.005.
[41] Dai H, Xu H. Selective and sensitive fluorescent chemosensors for Cu^{2+} ion based upon Bis-1,8-naphthalimide dyads. Chin J Chem 2012;30:267–72. https://doi.org/10.1002/cjoc.201180481.
[42] Lide David, ed., CRC handbook of chemistry and physics, 85th ed., CRC press.
[43] Yang X-Q, Yang L-J, Huang K-M, Tian W-Y, Shang H. Experimental and the theoretical studies of the dielectric properties of DMSO–H2O mixtures. J Solut Chem 2010;39:849–56. https://doi.org/10.1007/s10953-010-9543-8.
[44] Greiner R, Schlücker T, Zgela D, Langhals H. Fluorescent aryl naphthalene dicarboximides with large stokes shifts and strong solvatochromism controlled by dynamics and molecular geometry. J Mater Chem C 2016;4:11244–52. https://doi.org/10.1039/C6TC04453K.
[45] Mahdiani M, Rouhani S, Zahedi P. Synthesis, solvatochromism and fluorescence quenching studies of naphthalene diimide dye by nano graphene oxide. J Fluoresc 2023;33:2003–14. https://doi.org/10.1007/s10895-023-03197-0.
[46] Reichardt C. Solvatochromic dyes as solvent polarity indicators. Chem Rev 1994;94:2319–58. https://doi.org/10.1021/cr00032a005.
[47] Felip-León C, Galindo F, Miravet JF. Insights into the aggregation-induced emission of 1,8-naphthalimide-based supramolecular hydrogels. Nanoscale 2018;10:17060–9. https://doi.org/10.1039/C8NR03755H.
[48] Srivastava AK, Singh A, Mishra L. Tuning of aggregation enhanced emission and solid state emission from 1,8-Naphthalimide derivatives: Nanoaggregates, spectra, and DFT calculations. J Phys Chem A 2016;120:4490–504. https://doi.org/10.1021/acs.jpca.6b05355.
[49] Yu X, Xie D, Lan H, Li Y, Zhen X, Ren J, Yi T. Effect of water on the supramolecular assembly and functionality of a naphthalimide derivative: tunable honeycomb structure with mechanochromic properties. J Mater Chem C 2017;5:5910–6. https://doi.org/10.1039/C7TC01331K.
[50] Misra S, Singh P, Das A, Brandão P, Sahoo P, Sepay N, Bhattacharjee G, Datta P, Mahapatra AK, Satpati B, Nanda J. Supramolecular assemblies of a 1,8-naphthalimide conjugate and its aggregation-induced emission property. Mater Adv 2020;1:3532–8. https://doi.org/10.1039/D0MA00584C.
[51] Das RJ, Mahata K. Mutualistic benefit in the self-sorted co-aggregates of *peri* -naphthoindigo and a 4-amino-1,8-naphthalimide derivative. Soft Matter 2019;15:5282–6. https://doi.org/10.1039/C9SM00454H.
[52] Marullo S, Feroci M, Noto R, D'Anna F. Insights into the anion effect on the self assembly of perylene bisimide diimidazolium salts. Dyes Pigments 2017;146. https://doi.org/10.1016/j.dyepig.2017.06.051.
[53] Heyne B. Self-assembly of organic dyes in supramolecular aggregates. Photochem Photobiol Sci 2016;15:1103–14. https://doi.org/10.1039/c6pp00221h.
[54] Chen Z, Lohr A, Saha-Möller CR, Würthner F. Self-assembled π-stacks of functional dyes in solution: structural and thermodynamic features. Chem Soc Rev 2009;38:564–84. https://doi.org/10.1039/B809359H.
[55] Smulders MMJ, Nieuwenhuizen MML, de Greef TFA, van der Schoot P, Schenning APHJ, Meijer EW. How to distinguish isodesmic from cooperative supramolecular polymerisation. Chem Eur J 2010;16:362–7. https://doi.org/10.1002/chem.200902415.
[56] D'Anna F, Marullo S, Lazzara G, Vitale P, Noto R. Aggregation processes of perylene bisimide diimidazolium salts. Chem Eur J 2015;21. https://doi.org/10.1002/chem.201502240.
[57] Tanwar AS, Meher N, Adil LR, Iyer PK. Stepwise elucidation of fluorescence based sensing mechanisms considering picric acid as a model analyte. Analyst 2020;145:4753–67. https://doi.org/10.1039/D0AN00732C.
[58] Chen S, Yu Y-L, Wang J-H. Inner filter effect-based fluorescent sensing systems: a review. Anal Chim Acta 2018;999:13–26. https://doi.org/10.1016/j.aca.2017.10.026.
[59] Liu J, de Silva AP. Path-selective photoinduced electron transfer (PET) in a membrane-associated system studied by pH-dependent fluorescence. Inorg Chim Acta 2012;381:243–6. https://doi.org/10.1016/j.ica.2011.09.059.
[60] Georgiev NI, Bojinov VB. Design, synthesis and sensor activity of a highly photostable blue emitting 1,8-naphthalimide. J Lumin 2012;132:2235–41. https://doi.org/10.1016/j.jlumin.2012.04.023.
[61] Zheng S, Lynch PLM, Rice TE, Moody TS, Gunaratne HQN, de Silva AP. Structural effects on the pH-dependent fluorescence of naphthalenic derivatives and consequences for sensing/switching. Photochem Photobiol Sci 2012;11:1675–81. https://doi.org/10.1039/c2pp25069a.

[62] Kelly LA, Roll M, Joseph J, Seenisamy J, Barrett J, Kauser K, Warner KS. Solvent-dependent photophysics and reactivity of monomeric and dimeric 4-Amino-1,8-Naphthalimides. J Phys Chem A 2021;125:2294–307. https://doi.org/10.1021/acs.jpca.0c11639.
[63] Georgiev NI, Dimitrova MD, Todorova YD, Bojinov VB. Synthesis, chemosensing properties and logic behaviour of a novel ratiometric 1,8-naphthalimide probe based on ICT and PET. Dyes Pigments 2016;131:9–17. https://doi.org/10.1016/j.dyepig.2016.03.051.
[64] Molina-García L, Santos JLM, Ruiz-Medina A, Llorent-Martínez EJ. Determination of ketoprofen based on its quenching effect in the fluorescence of quantum dots. J Food Drug Anal 2013;21:426–31. https://doi.org/10.1016/j.jfda.2013.09.007.
[65] Romano GM, Mummolo L, Savastano M, Paoli P, Rossi P, Prodi L, Bencini A. Polyamine receptors containing anthracene as fluorescent probes for ketoprofen in H_2O/EtOH solution. Chem Commun 2022;58:7022–5. https://doi.org/10.1039/D2CC01107G.
[66] Chandel P, Sharma S, Mohiuddin I, Bhogal S. Mesoporous silica-encapsulated nitrogen-doped fluorescent carbon dots modified polydopamine composites for monitoring non-steroidal anti-inflammatory drugs. Microchem J 2024;204:111000. https://doi.org/10.1016/j.microc.2024.111000.
[67] Bhogal S, Kaur K, Maheshwari S, Malik AK. Surface molecularly imprinted carbon dots based core-shell material for selective fluorescence sensing of ketoprofen. J Fluoresc 2019;29:145–54. https://doi.org/10.1007/s10895-018-2322-4.
[68] Duan L, Zhao Y. Molecularly imprinted micelles for fluorescent sensing of nonsteroidal anti-inflammatory drugs (NSAIDs). React Funct Polym 2021;158:104759. https://doi.org/10.1016/j.reactfunctpolym.2020.104759.
[69] Mudliar NH, Dongre PM, Singh PK. An efficient J-aggregate based fluorescence turn-on and ratiometric sensor for heparin. Sensor Actuator B Chem 2019;301:127089. https://doi.org/10.1016/j.snb.2019.127089.
[70] Bhaumik SK, Patra YS, Banerjee S. High affinity heparin detection by multivalent supramolecular polymers through aggregation induced emission. Chem Commun 2020;56:9541–4. https://doi.org/10.1039/D0CC03644G.